研究成果の刊行に関する一覧表

雑誌

発表者氏名	論文タイトル名	発表誌名	巻号	ページ	出版年
Asai, T., Miyazawa, S., Maeda, N., Hatanaka, K., Katanasaka, Y., Shimizu, K., Shuto, S., Oku, N.	Antineovascular therapy with angiogenic vessel-targeted polyethyleneglycol-shielded liposomal DPP-CNDAC.	*Cancer Sci.*			in press
Asai, T., Suzuki, Y., Matsushita, S., Yonezawa, S., Yokota, J., Katanasaka, Y., Ishida, T., Dewa, T., Kiwada, H., Nango, M., Oku, N.	Disappearance of the angiogenic potential of endothelial cells caused by Argonaute2 knockdown.	*Biochem. Biophys. Res. Commun.*	368	243-248	2008
Shimizu, K., Sawazaki, Y., Tanaka, T., Asai, T., Oku, N.	Chronopharmacologic cancer treatment with an angiogenic vessel-targeted liposomal drug.	*Biol. Pharm. Bull.*	31	95-98	2008
Shiraga, E., Barichello, J.M., Ishida, T., Kiwada, H.,	A metronomic schedule of cyclophosphamide combined with PEGylated liposomal doxorubicin has a highly antitumor effect in an experimental pulmonary metastatic mouse model.	*Int. J. Pharm.*	353	65-73	2008
Hatakeyama, H., Akita, H., Ishida, E., Hashimoto, K., Kobayashi, H., Aoki, T., Yasuda, J., Obata, K., Kikuchi, K., Ishida, T., Kiwada, H., Harashima, H.	Tumor targeting of doxorubicin by anti MT1-MMP antibody-modified PEG liposomes.	*Int. J. Pharm.*	342	194-200	2007
Atobe K., Ishida T., Ishida, E., Hashimoto K., Kobayashi H., Yasuda J., Aoki, T., Obata K, Kikuchi H., Akita, H., Asai, T, Harashima, H., Oku, N., Kiwada, H.	In vitro efficacy of a sterically stabilized immunoliposomes targeted to membrane type 1 matrix metalloproteinase (MT1-MMP).	*Biol. Pharm. Bull.*	30	972-978	2007
Katanasaka, Y., Asai, T., Naitou, H., Ohashi, N., Oku, N.	Proteomic characterization of angiogenic endothelial cells stimulated with cancer cell-conditioned medium.	*Biol. Pharm. Bull.*	30	2300-2307	2007
Ishida, T., Wang X.Y., Shimizu, T., Nawata, K., Kiwada, H.	PEGylated liposomes elicit an anti-PEG IgM response in a T-cells independent manner.	*J. Control. Release*	122	349-355	2007

Antineovascular therapy with angiogenic vessel-targeted polyethyleneglycol-shielded liposomal DPP–CNDAC

Tomohiro Asai,[1] Souichiro Miyazawa,[1] Noriyuki Maeda,[1,2] Kentaro Hatanaka,[1] Yasufumi Katanasaka,[1] Kosuke Shimizu,[1] Satoshi Shuto[3] and Naoto Oku[1,4]

[1]Department of Medical Biochemistry and Global COE, University of Shizuoka School of Pharmaceutical Sciences, 52-1 Yada, Suruga-ku, Shizuoka 422-8526; [2]*Nippon Fine Chemical Co. Ltd, Takasago, Hyogo 676-0074;* [3]Faculty of Pharmaceutical Sciences, Hokkaido University, Kita-12, Nishi-6, Kita-ku, Sapporo 060-0812, Japan

(Received September 6, 2007/Revised December 29, 2007/Accepted January 7, 2008)

Causing damage to angiogenic vessels is a promising approach for cancer chemotherapy. The present study is a codification of a designed liposomal drug delivery system (DDS) for antineovascular therapy (ANET) with 2′-C-cyano-2′-deoxy-1-β-D-*arabino*-pentofuranosylcytosine (CNDAC). The authors have previously reported that liposomalized 5′-*O*-dipalmitoylphosphatidyl CNDAC (DPP–CNDAC), a phospholipid derivative of the novel antitumor nucleoside CNDAC, is quite useful for ANET. DPP–CNDAC liposomes modified with APRPG, a peptide having affinity toward angiogenic vessels, efficiently suppressed tumor growth by damaging angiogenic endothelial cells. In the present study, the authors masked the hydrophilic moiety of DPP–CNDAC, namely, CNDAC, on the liposomal surface with APRPG–polyethyleneglycol (PEG) conjugate to improve the availability of DPP–CNDAC liposomes. The use of the APRPG–PEG conjugate attenuated the negative ζ-potential of the DPP–CNDAC liposomes and reduced the agglutinability of them in the presence of serum. These effects improved the blood level of DPP–CNDAC liposomes in colon 26 NL-17 tumor-bearing BALB/c male mice, resulting in enhanced accumulation of them in the tumor. Laser scanning microscopic observations indicated that APRPG–PEG-modified DPP–CNDAC liposomes (LipCNDAC/APRPG–PEG) colocalized with angiogenic vessels and strongly induced apoptosis of tumor cells, whereas PEG-modified DPP–CNDAC liposomes (LipCNDAC/PEG) did not. In fact, LipCNDAC/APRPG–PEG suppressed the tumor growth more strongly compared to LipCNDAC/PEG and increased significantly the life span of the mice. The present study is a good example of an effective liposomal DDS for ANET that is characterized by: (i) phospholipid derivatization of a certain anticancer drug to suit the liposomal formulation; (ii) PEG-shielding for masking undesirable properties of the drug on the liposomal surface; and (iii) active targeting to angiogenic endothelial cells using a specific probe. (*Cancer Sci* 2008)

Because the inhibition of angiogenesis suppresses tumor growth and hematogenous metastases, antiangiogenic therapies have been widely investigated.[1–3] These therapies are also expected to be effective toward a broad spectrum of cancers, including drug-resistant cancers. Besides antiangiogenic therapy, ANET, namely, the causing of indirect lethal damage to tumor cells by the complete cut-off of the supply of oxygen and nutrients through damaging neovessels, is being developed.[4,5] For ANET, the authors previously isolated from a phage-displayed peptide library a peptide that specifically binds to the tumor angiogenic vasculature. The epitope sequence of the peptide was determined to be APRPG.[6,7] The authors demonstrated that APRPG is a useful probe for the active targeting of angiogenic vessels, although the target molecule of APRPG is still unknown. In contrast, PEG-coating of liposomes has been used in a liposomal DDS. It is known that PEG-modified liposomes characteristically remain in the circulation longer than non-modified ones through avoidance of RES-trapping of drug carriers.[8–10] PEG modification of the liposomal surface is known to form a fixed aqueous layer around the liposome due to the interaction between the PEG-polymer and water molecules, and thus prevents the binding of certain serum proteins and opsonins that are responsible for RES-trapping.[11] The feature of long circulation causes liposomal accumulation in tumor tissues, because the angiogenic vasculature in tumor tissues is quite leaky and macromolecules easily accumulate in the interstitial tissues of the tumor due to the EPR effect.[12,13] In the case of ANET, this long time in circulation increases the opportunity for specific binding of ligand-modified liposomes to angiogenic vessels. For this purpose, the authors previously designed a compound composed of APRPG, PEG, and DSPE.[14,15] It has been demonstrated that APRPG–PEG modification is superior to just APRPG modification for enhancing the antitumor activity of liposomal doxorubicin.[16]

In the present study, the authors used CNDAC as a chemotherapeutic agent. CNDAC had been originally synthesized as a novel antitumor nucleoside anti-metabolite by Matsuda *et al.*, who showed that CNDAC has a novel anticancer mechanism and induces DNA strand breaks after its incorporation into tumor cell DNA.[17] The results of phase I clinical studies of its N4-palmitoyl derivative (CS-682) in patients with malignant solid tumors were reported recently.[18,19] The authors previously designed DPP–CNDAC for liposomalization,[20] because liposomal drugs show improved biodistribution and bioavailability in tumor-bearing animals. In fact, liposomal DPP–CNDAC showed enhanced activities for reducing tumor growth and increasing the life span of mice than conventional liposomes or soluble CNDAC.[21,22] As the next step, DPP–CNDAC liposomes were modified with APRPG for the purpose of ANET. APRPG-modification of DPP–CNDAC liposomes actually caused effective tumor growth suppression, possibly through damaging angiogenic endothelial cells.[23] These results also indicated that the therapeutic efficacy should reflect the damage to the angiogenic endothelial cells to which the liposomes gain access, because lipophilic drugs should be delivered to the cells in a liposomal form. However, the *in vivo* behavior of APRPG-modified DPP–CNDAC

[4]To whom correspondence should be addressed. E-mail: oku@u-shizuoka-ken.ac.jp

Abbreviations: ANET, antineovascular therapy; APRPG, Ala-Pro-Arg-Pro-Gly; BSA, bovine serum albumin; CNDAC, 2′-C-cyano-2′-deoxy-1-β-D-*arabino*-pentofuranosylcytosine; DDS, drug delivery system; $DiIC_{18}$, 1,1′-dioctadecyl-3,3,3′,3′,-tetramethylindo-carbocyanine perchlorate; DPPC, dipalmitoylphosphatidylcholine; DPP–CNDAC, 5′-*O*-dipalmitoylphosphatidyl–CNDAC; DSPC, distearoylphosphatidylcholine; DSPE, distearoylphosphatidylethanolamine; EPR, enhanced permeability and retention; FBS, fetal bovine serum; FITC, fluoroscein-5-isothiocyanate, LipCNDAC, DPP–CNDAC liposomes; LipCNDAC/APRPG–PEG, APRPG–PEG-modified DPP–CNDAC liposomes; LipCNDAC/PEG, PEG-modified DPP–CNDAC liposomes; PBS, phosphate-buffered saline; PEG, polyethyleneglycol; RES, reticuloendothelial system; TUNEL, terminal dUTP nick end labeling.

doi: 10.1111/j.1349-7006.2008.00758.x

liposomes was affected by the presence of the cyano group of DPP–CNDAC on the liposomal surface. It induced aggregation of liposomes, resulting in reduced blood circulation of liposomes.

In the present study, the CNDAC on the liposomal surface was masked with APRPG–PEG conjugate to erase this undesirable property of DPP–CNDAC in liposomalization. The authors integrated their previous observations to formulate angiogenic vessel-targeted long-circulating DPP–CNDAC liposomes and applied them to ANET.

Materials and Methods

Materials. Synthesis of CNDAC and DPP–CNDAC was performed as described previously.[17,20] A phosphatidyl group was introduced into CNDAC through transphosphatidylation from 1,2-dipalmitoyl-3-sn-glycerophosphocholine using phospholipase D. Preparation of DSPE–PEG and DSPE–PEG–APRPG was performed as described previously.[14] DSPC and cholesterol were obtained from Nippon Fine Chemical Co., Ltd (Takasago, Hyogo, Japan). Colon 26 NL-17 colon carcinoma cells were established by Dr Yamori (Japanese Foundation for Cancer Research, Tokyo, Japan) and kindly provided by Dr Nakajima (Johnson & Johnson KK, Tokyo, Japan).

Animals. Five-week-old BALB/c male mice were obtained from Japan SLC Inc. (Shizuoka, Japan). The animals were cared for according to the animal facility guidelines of the University of Shizuoka.

Preparation of liposomes. DPP–CNDAC, DSPC, and cholesterol with DSPE–PEG (LipCNDAC/PEG) or DSPE–PEG–APRPG (LipCNDAC/APRPG–PEG) (10:10:5:2 as a molar ratio), or DPP–CNDAC, DSPC, and cholesterol without PEG-conjugate (LipCNDAC, 10:10:5 as a molar ratio) were dissolved in chloroform/methanol, dried under reduced pressure, and stored *in vacuo* for at least 1 h. Liposomes were produced by hydration of a thin lipid film with 10 mM phosphate-buffered 0.3 M sucrose (pH 6.8), and frozen and thawed for three cycles using liquid nitrogen. Then the liposomes were sized by extrusion thrice through polycarbonate membrane filters with 100-nm-diameter pores (Nucleopore, Maidstone, UK). The liposomal solutions were centrifuged at 180 000*g* for 20 min (CS120EX, Hitachi, Japan) to remove the untrapped DPP–CNDAC if present. Then the liposomes were resuspended in 10 mM phosphate-buffered 0.3 M sucrose. To determine the efficacy of trapping DPP–CNDAC in the liposomes, an aliquot of the liposomal solution was solubilized by the addition of reduced Triton X-100 (Sigma-Aldrich Co., St Louis, MO, USA), and the amount of DPP–CNDAC was optically determined at 280 nm after the pH of the solution had been adjusted to 1.0. For a biodistribution study, a trace amount of [1α, 2α(n)-^{3}H] cholesterol oleoyl ether (74 kBq/mouse, Amersham Pharmacia, Buckinghamshire, England) was added to the initial organic solution. To examine the intratumoral localization of liposomes in tumor syngrafts, $DiIC_{18}$ (Molecular Probes Inc., Eugene, OR, USA) was added to the initial organic solution (DPP–CNDAC:DSPC: cholesterol:$DiIC_{18}$:DSPE–PEG or DSPE–PEG–APRPG = 10:10:5:0.1:2; DPP–CNDAC : DSPC : cholesterol : $DiIC_{18}$ = 10:10:5:0.1, as a molar ratio). For the therapeutic study, control liposomes composed of DPPC, DSPC, and cholesterol (10:10:5 as a molar ratio) were prepared similarly as for the other liposomes.

Characterization of liposomes. Particle size and ζ-potential of liposomes diluted with PBS(–) were measured using a Zetasizer Nano ZS (Malvern, Worcestershire, UK). Aggregation testing was performed as follows: The liposomal solution was incubated in PBS(–) or in the presence of 50% FBS (Sigma-Aldrich) at 37°C for 1 h. The turbidity of the liposomal solution was determined at 450 nm, and relative turbidity compared with that in 0.3 M sucrose was then calculated.

Biodistribution of liposomes. Colon 26 NL-17 cells were cultured in DME/F12 medium (Nissui, Tokyo, Japan) supplemented with 10% FBS (Sigma-Aldrich). After harvesting of the cells, 1.0×10^6 cells were carefully injected subcutaneously into the posterior flank of 5-week-old BALB/c male mice. The biodistribution study was performed when the tumor size had become approximately 10 mm in diameter. Size-matched colon 26 NL-17 carcinoma-bearing mice were injected with the radiolabeled liposomes containing [1α, 2α (n)-^{3}H] cholesterol oleoyl ether via a tail vein. One hour after the injection, the mice were killed under diethyl ether anesthesia for the collection of blood. The plasma was obtained by centrifugation (600*g* for 5 min). After the mice had been bled from the carotid artery, the heart, lung, liver, spleen, kidney, and tumor were removed, washed with saline, and weighed. The radioactivity in each organ was determined using a liquid scintillation counter (LSC-3100, Aloka, Tokyo, Japan). Distribution data were presented as percentage dose per gram of tissue or per 0.1 mL plasma. The total amount in plasma was calculated based on the average body weight of the mice, where the average plasma volume was assumed to be 4.27% of the body weight based on the data on total blood volume.

Histochemical analysis of liposomal distribution in tumor syngrafts. $DiIC_{18}$-labeled liposomes were administered via a tail vein of colon 26 NL-17 carcinoma-bearing mice when the tumor sizes had reached approximately 10 mm in diameter. Two hours after the injection of liposomes, the mice were bled from the carotid artery under diethyl ether anesthesia, and the tumors were dissected. Histochemical analysis was performed according to the method described previously.[16] In brief, solid tumors were embedded in optimal cutting temperature compound (Sakura Finetechnochemical Co. Ltd, Tokyo, Japan) and frozen at –80°C. Five-micrometer tumor sections were prepared using a cryostat microtome (HM 505E, Microm, Walldorf, Germany), mounted on MAS-coated slides (Matsunami Glass Ind., Ltd, Japan), and air-dried for 1 h. The tissue sections were then fixed with acetone, and washed twice with PBS(–). After the sections had been blocked with 1% BSA in PBS(–), they were incubated with biotinylated antimouse CD31 rat monoclonal antibody (Becton Dickinson Laboratory, Franklin Lakes, NJ, USA) for 18 h at 4°C and then visualized after incubation with streptavidin–FITC conjugates (Molecular Probes Inc., Eugene, OR, USA) for 30 min at room temperature in a humid chamber. These sections were observed for fluorescence using an LSM microscope system (Carl Zeiss, Co. Ltd, Jena, Germany).

Determination of apoptotic cells in tumors. LipCNDAC/PEG or LipCNDAC/APRPG–PEG was administered intravenously into colon 26 NL-17 tumor-bearing mice when the tumor size had reached approximately 10 mm in diameter. Twelve hours after injection of the liposomes, the tumors were dissected from the mice; and tumor sections were then prepared. Next, immunostaining of endothelial cells was performed as described above, except that streptavidin–Alexa 594 conjugate (Molecular Probes Inc.) was used as fluorescent dye instead of streptavidin–FITC conjugate. For visualizing apoptotic cells, TUNEL staining was performed using an ApopTag Plus Fluorescein *In Situ* Apoptosis Detection Kit (Intergen Co., Purchase, NY, USA) according to the recommended procedures supplied in the kit. In brief, tumor sections were washed and equilibrated for 15 min in a humid chamber at room temperature, and then reacted with TdT enzyme for 1 h at 37°C. Thereafter, they were stained with antidigoxigenin–fluorescein antibody, after which the sections were observed using the LSM system. Apoptotic signals (green signals) were analyzed using Image J software (NIH).

Therapeutic experiment. LipCNDAC/PEG, LipCNDAC/APRPG–PEG or control liposomes were administered intravenously into colon 26 NL-17 tumor-bearing mice. The injected dose for each administration was 15 mg/kg as CNDAC moiety. The treatment was started when the tumor volume became approx. 0.1 cm^3. The size of the tumor and the body weight of each mouse were

doi: 10.1111/j.1349-7006.2008.00758.x

monitored daily thereafter. Two bisecting diameters of each tumor were measured with slide calipers to determine the tumor volume. Calculation of the tumor volume was performed using the formula 0.4 ($a \times b^2$), where a is the largest and b is the smallest diameter. The calculated tumor volume correlated well with the actual tumor weight ($r = 0.980$).[24] The life spans of tumor-bearing mice were also monitored.

Statistical analysis. Variance in a group was evaluated using the F-test; and differences in mean tumor volume using Student's t-test.

Results

Characterization of DPP–CNDAC liposomes. The efficiency of entrapment of DPP–CNDAC into liposomes was approximately 100% in all experiments (data not shown). Because DPP–CNDAC was easily incorporated into the lipid bilayer of liposomes as a lipid component, the CNDAC moieties of DPP–CNDAC were speculated to be exposed on the liposomal surface. In fact, the ζ-potential of LipCNDAC was negative due to the presence of the cyano group in CNDAC (Table 1). In contrast, PEG- or APRPG–PEG-modification reduced the negativity of the ζ-potential of DPP–CNDAC liposomes, suggesting that PEG shielded CNDAC moieties on the liposomal surface by forming a fixed aqueous layer (Table 1). As shown in Fig. 1, the agglutinability of both LipCNDAC/PEG and LipCNDAC/APRPG–PEG in the presence of serum was considerably low compared with that of LipCNDAC.

Biodistribution study. The biodistribution of these three types of liposomes was determined in colon 26 NL-17 carcinoma-bearing mice. At 1 h after administration of these liposomes, the plasma concentrations of LipCNDAC/PEG and LipCNDAC/APRPG–PEG were significantly higher than that of LipCNDAC (Fig. 2). These data suggest that the use of PEG or APRPG–PEG reduced the aggregation of these liposomes in the blood circulation, which prevented recognition of them by RES and endowed them with long circulation. In addition, APRPG–PEG modification significantly improved the blood circulation of DPP–CNDAC liposomes at 3 or 24 h administration of these liposomes (data not shown). Therefore, LipCNDAC/PEG and LipCNDAC/APRPG–PEG showed high accumulation in the tumors compared with LipCNDAC, possibly through the EPR effect. Particularly in LipCNDAC/APRPG–PEG, this characteristic of long circulation would increase the opportunity for specific binding of these liposomes to angiogenic vessels.

Histochemical analysis of the tumor. Colon 26 NL-17-bearing mice were given a single i.v. dose of LipCNDAC/PEG or LipCNDAC/APRPG–PEG. As shown in Fig. 3a–c, when the fluorescently labeled LipCNDAC/PEG was injected, the liposomal distribution (red fluorescence) was observed to be separate from endothelial cells (green fluorescence). In contrast, LipCNDAC/APRPG–PEG was colocalized with endothelial cells (Fig. 3d–f). These data suggest that LipCNDAC/APRPG–PEG became selectively localized on angiogenic endothelial cells. Cellular

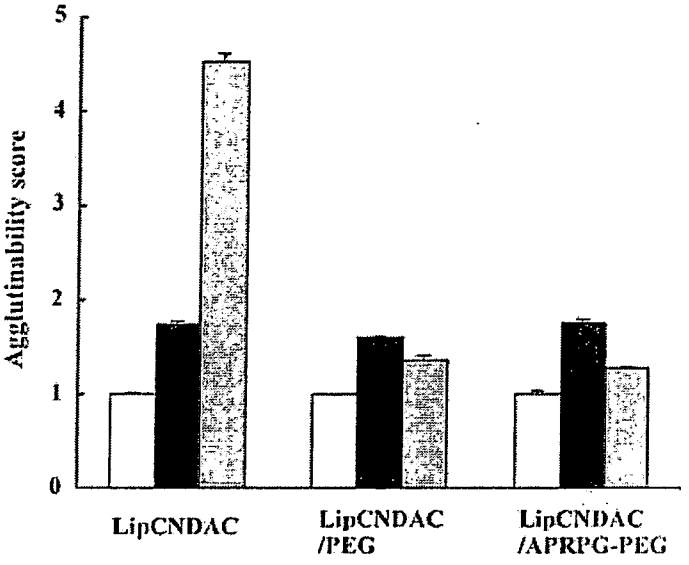

Fig. 1. Aggregation of DPP–CNDAC liposomes in the presence of serum. LipCNDAC, LipCNDAC/PEG or LipCNDAC/APRPG–PEG was incubated in (□) 10 mM phosphate-buffered 0.3 M sucrose, (■) PBS(–) or (▨) 50% FBS at 37°C for 1 h. The turbidity of the solutions was measured by absorption at 450 nm. The turbidity of the PBS or the FBS group relative to that of the sucrose group is shown, along with SD bars. Similar results were obtained in separate experiments. APRPG, Ala-Pro-Arg-Pro-Gly; CNDAC, 2′-*C*-cyano-2′-deoxy-1-β-D-*arabino*-pentofuranosylcytosine; DPP, 5′-*O*-dipalmitoylphosphatidyl; FBS, fetal bovine serum; LipCNDAC, DPP–CNDAC liposomes; PBS, phosphate-buffered saline; PEG, polyethyleneglycol.

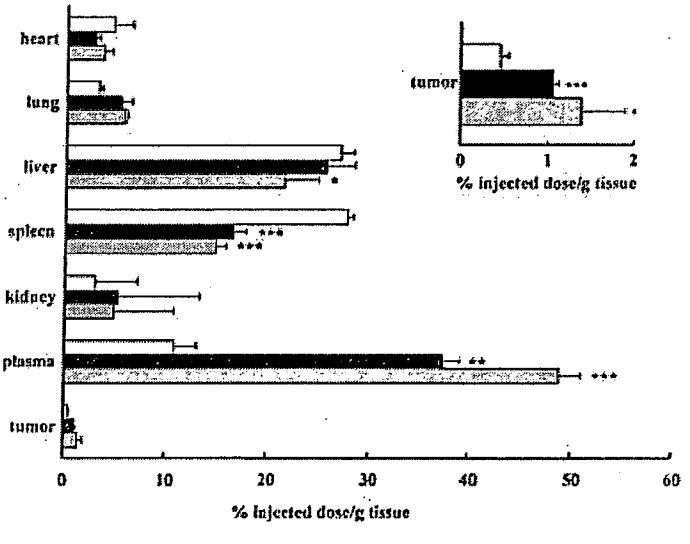

Fig. 2. Biodistribution of DPP–CNDAC liposomes in tumor-bearing mice. Liposomes were prepared and radiolabeled as described in Materials and Methods. Size-matched colon 26 NL-17 carcinoma-bearing mice ($n = 4$) were injected with (□) LipCNDAC, (■) LipCNDAC/PEG or (▨) LipCNDAC/APRPG–PEG, at 15 mg/kg as CNDAC, into a tail vein. One hour after injection, these mice were killed under diethyl ether anesthesia and each organ was dissected. The radioactivity in the plasma and each organ was determined in a liquid scintillation counter. Data are presented as the amount incorporated as a percentage of the injected dose per gram of tissue and SD in each tissue. (In the case of plasma, the value was per 0.1 mL instead of per gram). Significant differences from LipCNDAC are indicated ($^*P < 0.05$; $^{**}P < 0.01$; $^{***}P < 0.001$). APRPG, Ala-Pro-Arg-Pro-Gly; CNDAC, 2′-*C*-cyano-2′-deoxy-1-β-D-*arabino*-pentofuranosylcytosine; DPP, 5′-*O*-dipalmitoylphosphatidyl; LipCNDAC, DPP–CNDAC liposomes; PEG, polyethyleneglycol.

Table 1. Size and ζ-potential of DPP–CNDAC liposomes

	Size ± SD (nm)	ζ-potential (mV)
LipCNDAC	120.8 ± 3.5	−29.2
LipCNDAC/PEG	121.5 ± 5.7	−6.1
LipCNDAC/APRPG–PEG	102.4 ± 2.2	−3.6

Particle size and ζ-potential of DPP–CNDAC liposomes diluted with phosphate-buffered saline(–) were measured using a Zetasizer Nano ZS. APRPG, Ala-Pro-Arg-Pro-Gly; CNDAC, 2′-*C*-cyano-2′-deoxy-1-β-D-*arabino*-pentofuranosylcytosine; DPP, 5′-*O*-dipalmitoylphosphatidyl; LipCNDAC, DPP–CNDAC liposomes; LipCNDAC/APRPG–PEG, APRPG–PEG-modified DPP–CNDAC liposomes; LipCNDAC/PEG, PEG-modified DPP–CNDAC liposomes; PEG, polyethyleneglycol.

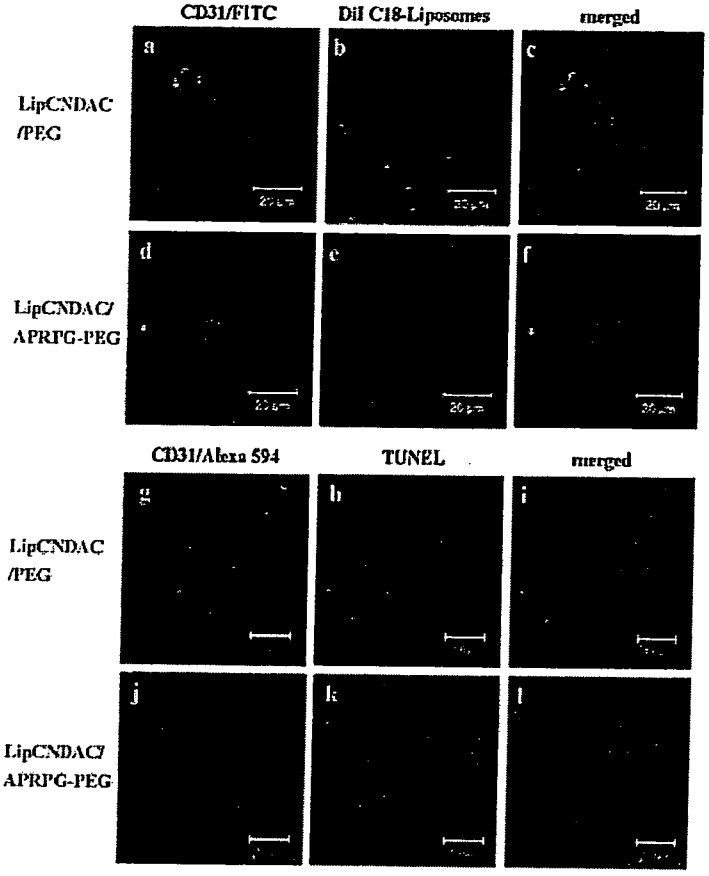

Fig. 3. Histochemical analysis of the tumor after injection of DPP–CNDAC liposomes. Size-matched colon 26 NL-17 carcinoma-bearing mice were injected i.v. with (a–c) LipCNDAC/PEG or (d–f) LipCNDAC/APRPG–PEG, at 15 mg/kg as CNDAC, on day 12 after tumor implantation. Two hours after the injection, each tumor was dissected and frozen sections were prepared. (a,d) Immunofluorescence staining for CD31 with FITC (green), and (b,e) liposomes labeled with $DiIC_{18}$ (red) are shown. (c,f) The merged images. The yellow portions indicate localization of liposomes at the site of vascular endothelial cells. In the experiment assessing apoptosis, colon 26 NL-17 carcinoma-bearing mice were similarly treated with (g–i) LipCNDAC/PEG or (j–l) LipCNDAC/APRPG–PEG. At 12 h after the injection, each tumor was dissected and frozen-sections were prepared. (g,j) The results of immunofluorescence staining for CD31 with Alexa 594 (red) and (h,k) TUNEL staining of apoptotic cells (green) are shown. (i,l) The merged images. APRPG, Ala-Pro-Arg-Pro-Gly; CNDAC, 2′-*C*-cyano-2′-deoxy-1-β-D-*arabino*-pentofuranosylcytosine; DPP, 5′-*O*-dipalmitoylphosphatidyl; LipCNDAC, DPP–CNDAC liposomes; FITC, fluoroscein-5-isothiocyanate; PEG, polyethyleneglycol; TUNEL, terminal dUTP nick end labeling.

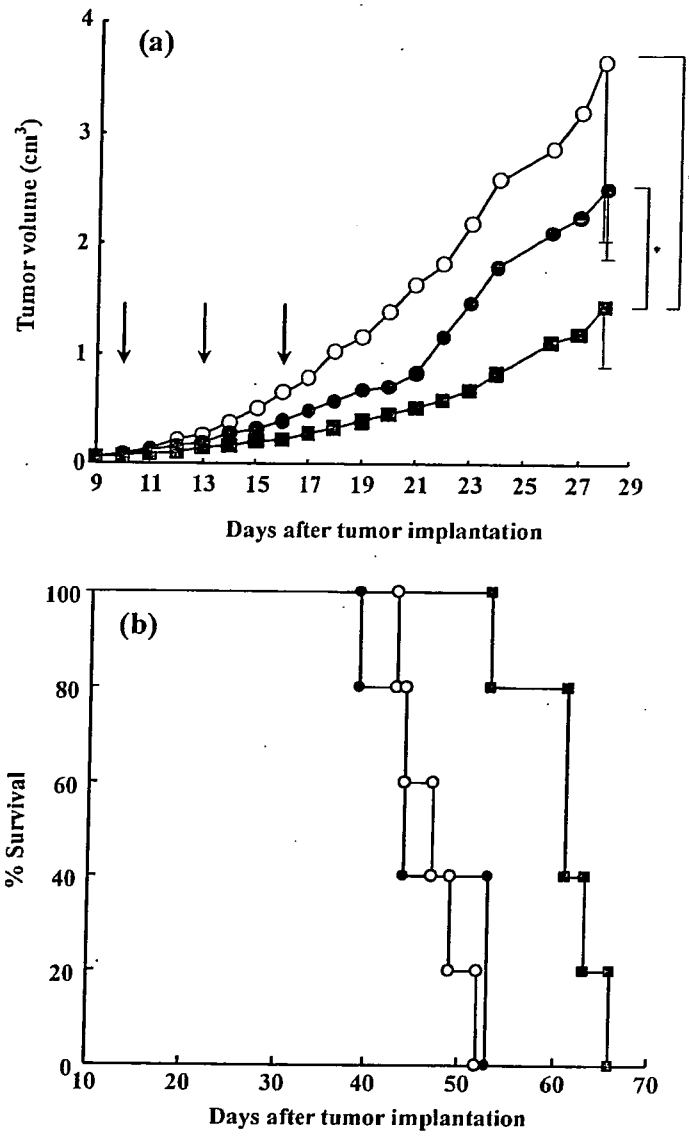

Fig. 4. Therapeutic efficacy of LipCNDAC/APRPG–PEG in tumor-bearing mice. Five-week-old BALB/c male mice (5 or 6 per group) were implanted s.c. with colon 26 NL-17 carcinoma cells into their left posterior flank. They were injected i.v. with (○) control liposomes, (●) LipCNDAC/PEG or (■) LipCNDAC/APRPG–PEG at 15 mg/kg as CNDAC on (→) days 10, 13, and 16 after tumor implantation. (a) The tumor volume and (b) survival time of mice were monitored to evaluate the therapeutic efficacy of DPP–CNDAC liposomes. Significant differences from the control liposome-treated group are indicated (*$P < 0.05$). APRPG, Ala-Pro-Arg-Pro-Gly; CNDAC, 2′-*C*-cyano-2′-deoxy-1-β-D-*arabino*-pentofuranosylcytosine; DPP, 5′-*O*-dipalmitoylphosphatidyl; LipCNDAC, DPP–CNDAC liposomes; PEG, polyethyleneglycol.

apoptosis in the tumor tissues was evaluated 12 h after administration of the liposomes (Fig. 3g–l). The signals of apoptotic cells were approximately 4.6-fold greater for LipCNDAC/APRPG–PEG than for LipCNDAC/PEG. CD31-staining did not show any vessel-like structure in the tumor of either liposome-treated group, suggesting that LipCNDAC/PEG also damaged angiogenic endothelial cells to some degree. These results indicate that LipCNDAC/APRPG–PEG had preferentially damaged angiogenic endothelial cells that induced effective apoptosis of tumor cells surrounding the damaged vessels.

Therapeutic efficacy of LipCNDAC/APRPG–PEG in tumor-bearing mice. LipCNDAC/APRPG–PEG suppressed tumor growth more efficiently than LipCNDAC/PEG: Significant differences in the tumor volume of the LipCNDAC/APRPG–PEG-treated group from that of the LipCNDAC/PEG-treated group were observed from day 22–28, although the SD data are shown only for day 28 (Fig. 4a). In addition, the tumor volume of the LipCNDAC/APRPG–PEG-treated group was significantly different from that of the control liposome-treated group from day 20–28. The body-weight change, an indicator of side-effects, was not observed in either the LipCNDAC/PEG- or LipCNDAC/APRPG–PEG-treated groups (data not shown). Corresponding to the tumor growth suppression, treatment with LipCNDAC/APRPG–PEG elongated the survival time of the mice: The mean survival times of the control liposomes, LipCNDAC/PEG-, and LipCNDAC/APRPG–PEG-treated groups were 47.6 ± 3.7, 46.6 ± 6.2, and 60.8 ± 4.8 days, respectively (Fig. 4b). The survival time of the LipCNDAC/APRPG–PEG-treated group was significantly longer than that for the mice treated with the control liposomes ($P < 0.001$) or LipCNDAC/PEG ($P < 0.01$).

doi: 10.1111/j.1349-7006.2008.00758.x

Discussion

The use of a DDS for targeting tumors is a promising strategy particularly for drugs with severe side-effects such as those used in cancer chemotherapy. CNDAC was developed as an effective anticancer drug,[17] but has severe side-effects like other anticancer drugs. To design a targeting DDS, the authors previously derivatized CNDAC as a phospholipid mimetic[20] because it was readily incorporated into liposomes, the most widely used drug carrier for a DDS. This mimetic, DPP–CNDAC, was well suited to liposomalization for cancer treatment.[21,22]

For the active targeting strategy for delivery of anticancer drugs, angiogenic vessels were selected as a target organ and a novel type of antiangiogenic therapy, antineovascular therapy (ANET), was examined. Vascular targeting has become an interesting issue in DDS, because anticancer drugs or their carriers first meet angiogenic vessels before extravasation into the tumor tissue. The authors previously applied APRPG-modified liposomes for antineovascular therapy using DPP–CNDAC. Because lipophilic drugs should be delivered to the cells in a liposomal form, the therapeutic efficacy should reflect the damage to the cells to which the liposomes gain access rather than a change in the local concentration of the agent in the tumor tissue. If the therapeutic efficacy of APRPG-modified DPP–CNDAC liposomes is superior to that of non-modified liposomal DPP–CNDAC, such a result would suggest that the destruction of angiogenic endothelial cells is superior to the direct destruction of tumor cells for effective tumor treatment. The authors' previous results indicate that the delivery of DPP–CNDAC to angiogenic endothelial cells is, in fact, useful for the suppression of tumor growth.[23]

PEG-shielding of the liposomal surface should be useful for designing active targeting DDS as well as passive targeting. In the present study, the significant efficacy of APRPG–PEG-modified DPP–CNDAC liposomes for tumor growth suppression was shown. An important aspect of the present study is that PEGylation served for not only RES-avoidance but also construction of a practical liposomal formulation using a lipid-derivatized drug. When the liposomal surface is modified with anticancer drugs such as DPP–CNDAC, the fixed aqueous layer formed by PEG can mask the undesirable properties of such liposomes for DDS. Thus, the RES avoidance afforded by the use of PEG enhanced the accumulation of the liposomes in the tumor tissue, enabled targeting of angiogenic endothelial cells, and caused efficient damage to tumor cells. Therefore, APRPG–PEG-modified liposomal DPP–CNDAC caused efficient tumor growth suppression without severe side-effects.

The present study is a good example of liposomalization if the property of the objective compound is not suitable to liposomalize, and the technology used is applicable to other agents. The present study indicates the importance of designing drug, carrier, and therapeutic strategy in the development of DDS pharmaceutics.

Acknowledgments

This work was supported by a Grant-in-Aid for Scientific Research.

References

1 Folkman J. Fundamental concepts of the angiogenic process. *Curr Mol Med* 2003; **3**: 643–51.
2 Hanahan D, Weinberg RA. The hallmarks of cancer. *Cell* 2000; **100**: 57–70.
3 Kerbel RS. Antiangiogenic drugs and current strategies for the treatment of lung cancer. *Semin Oncol* 2004; **31**: 54–60.
4 Shimizu K, Asai T, Oku N. Antineovascular therapy, a novel antiangiogenic approach. *Exp Opin Ther Targets* 2005; **9**: 63–76.
5 Asai T, Oku N. Liposomalized oligopeptides in cancer therapy. *Meth Enzymol* 2005; **391**: 163–76.
6 Oku N, Asai T, Watanabe K *et al.* Antineovascular therapy using novel peptides homing to angiogenic vessels. *Oncogene* 2002; **21**: 2662–9.
7 Asai T, Nagatsuka M, Kuromi K *et al.* Suppression of tumor growth by novel peptides homing to tumor-derived new blood vessels. *FEBS Lett* 2002; **510**: 206–10.
8 Klibanov AL, Maruyama K, Torchilin VP, Huang L. Amphipathic polyethyleneglycols effectively prolong the circulation time of liposomes. *FEBS Lett* 1990; **268**: 235–7.
9 Lasic DD. Doxorubicin in sterically stabilized liposomes. *Nature* 1996; **380**: 561–2.
10 Sakakibara T, Chen FA, Kida H *et al.* Doxorubicin encapsulated in sterically stabilized liposomes is superior to free drug or drug-containing conventional liposomes at suppressing growth and metastases of human lung tumor xenografts. *Cancer Res* 1996; **56**: 3743–6.
11 Sadzuka Y, Nakade A, Hirama R *et al.* Effects of mixed polyethyleneglycol modification on fixed aqueous layer thickness and antitumor activity of doxorubicin containing liposome. *Int J Pharm* 2002; **238**: 171–80.
12 Matsumura Y, Maeda H. A new concept for macromolecular therapeutics in cancer chemotherapy: mechanism of tumoritropic accumulation of proteins and the antitumor agent SMANCS. *Cancer Res* 1986; **46**: 6387–92.
13 Muggia F. Doxorubicin-polymer conjugates. Further demonstration of the concept of enhanced permeability and retention. *Clin Cancer Res* 1999; **5**: 7–8.
14 Maeda N, Takeuchi Y, Takada M, Namba Y, Oku N. Synthesis of angiogenesis-targeted peptides and hydrophobized polyethylene glycol conjugate. *Bioorg Med Chem Lett* 2004; **14**: 1015–17.
15 Maeda N, Takeuchi Y, Takada M, Sadzuka Y, Namba Y, Oku N. Antineovascular therapy by use of tumor neovasculature-targeted long-circulating liposome. *J Control Release* 2004; **100**: 41–52.
16 Maeda N, Miyazawa S, Shimizu K *et al.* Enhancement of anticancer activity in antineovascular therapy is based on the intratumoral distribution of the active targeting carrier for anticancer drugs. *Biol Pharm Bull* 2006; **29**: 1936–40.
17 Matsuda A, Nakajima Y, Azuma A, Tanaka M, Sasaki T. Nucleosides and nucleotides. 100. 2′-*C*-cyano-2′-deoxy-1-β-D-*arabino*furanosyl-cytosine (CNDAC): design of a potential mechanism-based DNA-strand-breaking antineoplastic nucleoside. *J Med Chem* 1991; **34**: 2917–19.
18 Delaunoit T, Burch PA, Reid JM *et al.* A phase I clinical and pharmacokinetic study of CS-682 administered orally in advanced malignant solid tumors. *Invest New Drugs* 2006; **24**: 327–33.
19 Gilbert J, Carducci MA, Baker SD, Dees EC, Donehower R. A Phase I study of the oral antimetabolite, CS-682, administered once daily 5 days per week in patients with refractory solid tumor malignancies. *Invest New Drugs* 2006; **24**: 499–508.
20 Shuto S, Awano H, Shimazaki N, Hanaoka K, Matsuda A. Nucleosides and nucleotides. 150. Enzymatic synthesis of 5′-phosphatidyl derivatives of 1-(2′-*C*-cyano-2-deoxy-β-D-*arabino*-pentofuranosyl) cytosine (CNDAC) and their notable antitumor effects in mice. *Bioorg Med Chem Lett* 1996; **6**: 1021–4.
21 Asai T, Kurohane K, Shuto S *et al.* Antitumor activity of 5′-*O*-dipalmitoylphosphatidyl 2′-*C*-cyano-2′-deoxy-1-β-D-*arabino*-pentofuranosylcytosine is enhanced by long-circulating liposomalization. *Biol Pharm Bull* 1998; **21**: 766–71.
22 Asai T, Shuto S, Matsuda A, Kakiuchi T, Ohba H, Tsukada H *et al.* Targeting and anti-tumor efficacy of liposomal 5′-*O*-dipalmitoylphosphatidyl 2′-*C*-cyano-2′-deoxy-1-β-D-*arabino*-pentofuranosylcytosine in mice lung bearing B16BL6 melanoma. *Cancer Lett* 2001; **162**: 49–56.
23 Asai T, Shimizu K, Kondo M *et al.* Antineovascular therapy by liposomal DPP–CNDAC targeted to angiogenic vessels. *FEBS Lett* 2002; **520**: 167–70.
24 Oku N, Doi K, Namba Y, Okada S. Therapeutic effect of adriamycin encapsulated in long-circulating liposomes on Meth-A-sarcoma-bearing mice. *Int J Cancer* 1994; **58**: 415–19.

Available online at www.sciencedirect.com
ScienceDirect
Biochemical and Biophysical Research Communications 368 (2008) 243–248
BBRC
www.elsevier.com/locate/ybbr

Disappearance of the angiogenic potential of endothelial cells caused by Argonaute2 knockdown

Tomohiro Asai [a,*], Yuko Suzuki [a], Saori Matsushita [a], Sei Yonezawa [a], Junichi Yokota [a], Yasufumi Katanasaka [a], Tatsuhiro Ishida [b], Takehisa Dewa [c], Hiroshi Kiwada [b], Mamoru Nango [c], Naoto Oku [a]

[a] *Department of Medical Biochemistry and Global COE, University of Shizuoka School of Pharmaceutical Sciences, 52-1 Yada, Suruga-ku, Shizuoka 422-8526, Japan*
[b] *Department of Pharmacokinetics and Biopharmaceutics, Institute of Health Biosciences, The University of Tokushima, 1-78-1 Sho-machi, Tokushima 770-8505, Japan*
[c] *Materials Science and Engineering, Nagoya Institute of Technology, Gokiso-cho, Showa-ku, Nagoya 466-8555, Japan*

Received 5 January 2008
Available online 28 January 2008

Abstract

Argonaute2 (Ago2), a component protein of RNA-induced silencing complex, plays a central role in RNA interference. We focused on the involvement of Ago2 in angiogenesis. Human umbilical vein endothelial cells (HUVECs) stimulated with several growth factors such as vascular endothelial growth factor were used for angiogenesis assays. We applied polycation liposomes for transfection of small interfering RNA (siRNA) to determine the biological effects of siRNA for Ago2 (siAgo2) on HUVECs. The proliferation study indicated that siAgo2 significantly suppressed the growth of HUVECs compared with control siRNA. TUNEL staining showed a certain population of HUVECs treated with siAgo2 underwent apoptosis. Furthermore, the treatment with siAgo2 suppressed the tube formation of HUVECs and significantly reduced the length of the tubes. These present data demonstrate that siAgo2 inhibited indispensable events of angiogenesis *in vitro*. This is the first report suggesting that Ago2 is required for angiogenesis.

Keywords: Argonaute2; Angiogenesis; siRNA; Polycation liposomes

Double-stranded RNA (dsRNA) provokes sequence-specific gene silencing, commonly called RNA interference (RNAi) [1,2]. RNAi is a type of post-transcriptional gene silencing, and gene therapy using small interfering RNA (siRNA) is expected to be a novel treatment strategy [3]. For inducing RNAi, siRNA needs to be incorporated into an RNA-induced silencing complex (RISC). MicroRNAs (miRNAs), which are endogenous small non-coding RNAs that negatively regulate gene expression, are also incorporated into RISC for the cleavage or translational inhibition of the target mRNA [4]. Argonaute2 (Ago2) is a component protein of RISC and plays a central role in RNAi [5]. When a guide (antisense) strand of siRNAs or miRNA binds to its target mRNA, Ago2 expresses enzymatic activity to cleave the mRNA [6]. Ago2 is distinct from other Argonaute family members in the point that only Ago2-containing RISC is able to catalyze cleavage [5–7]. Ago2 is thus considered to be an indispensable protein for inducing RNAi. In addition, Ago2 cleaves the passenger strand of siRNAs, which facilitates the assembly of siRNAs into RISC [4,8]. On the other hand, Ago2-deficient mice show several developmental abnormalities such as a cardiac failure and a defect of neural tube closure [6]. Since these animals show an embryonic-lethal phenotype, Ago2 is essential for embryonic development.

Pathological angiogenesis is involved in diseases such as cancer [9]. Understanding of the mechanisms of angiogenesis

* Corresponding author. Fax: +81 54 264 5705.
E-mail address: asai@u-shizuoka-ken.ac.jp (T. Asai).

0006-291X/$ - see front matter © 2008 Elsevier Inc. All rights reserved.
doi:10.1016/j.bbrc.2008.01.074

leads to various antiangiogenic therapeutic modalities [10]. For instance, Avastin, a neutralizing antibody for vascular endothelial growth factor, is already used in clinical cancer chemotherapy [11]. While the participation of many proteins such as cytokines and signaling molecules in angiogenesis is well known, certain kinds of miRNAs have recently been shown to participate in angiogenesis [12]. Also, Dicer, a protein that cleaves long dsRNAs, is required for embryonic angiogenesis during mouse development [13]. Taken together, available information suggests that a miRNA system might be closely related to the regulation of angiogenesis. However, the involvement of Ago2 in angiogenesis is not known at all.

The present study is mainly focused on the possible involvement of Ago2, in addition to Dicer, in the regulation of angiogenesis. Our next concern is the application of Ago2 knockdown to antiangiogenic therapy. For establishment of RNAi therapy, a siRNA delivery system is quite important as well as a therapeutic target [14]. Polycation liposomes (PCLs), one of the non-viral types of vectors, possess the advantages of both cationic liposomes and polycations for gene delivery [15]. PCLs are simply prepared by modification of the liposomal surface with cetylated PEI (cetyl-PEI). Our previous study demonstrated that PCLs show various advantageous properties such as high transfection efficiency of plasmid DNA, low cytotoxicity, and applicability for *in vivo* use [15]. In this study, we optimized the formulation of PCLs for siRNA transfection and used such liposomes for analyzing the biological effects of Ago2 knockdown on angiogenesis.

Materials and methods

Preparation of siRNA/PCL complexes. Cetyl-PEI was synthesized as described previously [15]. Cholesterol was kindly provided by NFC Co. (Takasago, Hyogo, Japan). Dioleoylphosphatidylethanolamine (DOPE) was purchased from NOF Co. (Tokyo, Japan).

Cetyl-PEI, DOPE, and cholesterol (0.05:1:0.5 or 0 as a molar ratio) were dissolved in *tert*-butyl alcohol and freeze–dried. PCLs were produced by hydration of the lipid mixture with DEPC-treated RNase-free water. PCLs were sized by extruding them 10 times through a polycarbonate membrane filter having 100-nm pores. PCLs and siRNA solution were diluted with serum-free medium corresponding to the respective cell lines used. Then, PCLs and siRNA were mixed gently and incubated for 15 min at room temperature to form siRNA/PCLs complexes. The ratio of the nitrogen moiety of PCLs to the phosphate one of siRNA (*N/P* ratio) was varied from 18 to 30 for formulation screening. The particle size and ζ-potential of siRNA/PCLs complexes diluted with DEPC-treated water were measured by using a Zetasizer Nano ZS (Malvern, Worcs, UK). All siRNAs used in this study were purchased from Hokkaido System Science Co. (Hokkaido, Japan).

Cell cultures. HT1080 human fibrosarcoma cells (HT1080 cells) were cultured in DME/Ham F12 medium containing 10% fetal bovine serum (FBS; Sigma–Aldrich, St. Louis, MO), 100 U/ml penicillin (MP Biomedicals, Irvine, CA), and 100 μg/ml streptomycin (MP Biomedicals). HT1080 cells constitutively expressing EGFP (EGFP/HT1080 cells) had been previously established [16] and were cultured in the above medium supplemented with 100 μg/ml geneticin (Sigma–Aldrich). Human umbilical vein endothelial cells (HUVECs, Cambrex Bio Science Walkersville, Walkersville, MD) were cultured on gelatin-coated dishes containing endothelial growth medium-2 (EGM-2; Cambrex Bio Science Walkersville).

PCL-mediated transfection with siRNA. Cells were seeded and precultured overnight. The medium was then changed to fresh medium containing FBS but no antibiotics. Prepared siRNA/PCLs complexes (*N/P* ratio: 24 equiv) were added to the medium at a final concentration of 40 nM (as siRNA). After 4-h incubation, the siRNA/PCLs complexes were removed. These cells were subsequently incubated at 37 °C for additional periods of time as described for each experimental procedure.

Determination of the amount of siRNA taken into cells. The amounts of siRNA taken into cells were determined fluorometrically by using siRNA for Argonaute2 (siAgo2) labeled with 6-fluorescein-6-carboxamido hexanoate (FAM) at the 3′-terminal of its antisense strand. The nucleotide sequences of siAgo2 with a 2-nucleotide overhang (underline) were 5′-GCACGGAAGUCCAUCUGAAUU-3′ (sense) and 5′-UUCAGAUGGACUUCCGUGCUU-3′ (antisense). These sequences of siAgo2 correspond to the nucleotide region 1425–1443 and have been validated by G. Meister et al. [7].

HT1080 cells (3×10^4 cells/well) or HUVECs (5×10^4 cells/well) were seeded onto 24-well plates. After the cells had been cultured overnight, FAM-labeled siAgo2 (final concentration: 40 nM) in complex with PCLs was added to the cultures, which were then incubated for 4 h. The transfected cells were lysed with 2% reduced Triton X-100 containing protease inhibitors (2 mM PMSF, 200 μM leupeptin, 50 μg/mL aprotinin, and 100 μM pepstatin A). The fluorescent intensities of FAM were measured by using a spectrophotofluorometer (Wallac ARVO™ SX 1420 Multilabel Counter, Perkin-Elmer Life Sciences, Boston, MA) and corrected for protein amounts by using a BCA Protein Assay Reagent Kit (PIERCE Biotechnology, Rockford, IL) according to the manufacturer's instructions.

Evaluation of the RNAi efficiencies obtained with PCLs. The nucleotide sequences of the siRNA for EGFP (siEGFP) with a 2-nucleotide overhang (underline) were 5′-GGCUACGUCCAGGAGCGCACC-3′ (sense) and 5′-UGCGCUCCUGGACGUAGCCUU-3′ (antisense). The sequences of siEGFP correspond to the nucleotide region 118–141.

EGFP/HT1080 cells were seeded onto 24-well plates at the density of 6×10^4 cells/well and transfected with siEGFP complexed with PCLs. After these cells had been transfected, the cells were lysed at 48 h after culture. The fluorescence intensity of EGFP was measured with a spectrophotofluorometer and corrected for protein amounts. EGFP/HT-1080 cells were also transfected with siEGFP mixed with Lipofectamine™ 2000 (LFA2K, Invitrogen, Rockville, MD) according to the manufacturer's instructions. The transfection time schedule was similar to that used for the PCLs.

Cytotoxicity assay. EGFP/HT-1080 cells were seeded onto 96-well plates at the density of 1.2×10^4 cells/well and transfected with siEGFP. After 24-h incubation, Tetracolor ONE™ (Seikagaku, Tokyo, Japan) was added to each well in accordance with the manufacturer's instructions. The amount of formazan formed in 3 h was measured on a microplate reader (MTP-120, Corona Electric, Ibaraki, Japan) at a test wavelength of 492 nm and a reference wavelength of 630 nm.

RT-PCR. Total RNA was isolated by using an RNeasy Plus Mini Kit (Qiagen, Valencia, CA) at 8, 16 or 24 h post-transfection with siRNA. Complementary DNA was generated from total RNA samples (5 μg) by use of a Ready-To-Go T-primed First-Strand Kit (Amersham Biosciences, Piscataway, NJ). The PCR conditions were as follow: for Ago2, 94 °C for 5 min followed by 30 cycles of 94 °C for 30 s, 67 °C for 30 s, and 72 °C for 30 s and then 72 °C for 15 min; for β-actin and EGFP, 94 °C for 2 min followed by 20 cycles of 94 °C for 30 s, 55 °C for 30 s, and 72 °C for 1 min and then 72 °C for 10 min; and for GAPDH, 95 °C for 5 min followed by 20 cycles of 95 °C for 30 s, 60 °C for 30 s, and 72 °C for 1 min and then 72 °C for 10 min. The primers for Ago2 were 5′-TGAACAACATCCTGCTGCCCCAGGGC-3′ (sense) and 5′-TCATGTTCGATGCTGGCTGTCACGGAAGGG-3′ (antisense); for β-actin, 5′-TGACGGGGTCACCCACACTGTGCCCATCTA-3′ (sense) and 5′-CTAGAAGCATTTGCGGTGGACGATGGAGGG-3′ (antisense), for EGFP, 5′-TACGGCAAGCTGACCCTGAAGTTC-3′ (sense) and 5′-CGTCCTTGAAGAAGATGGTGCG-3′ (antisense); and for GAPDH, 5′-TGTTGCCATCAATGACCCCTTC-3′ (sense) and 5′-AGCATCGCCCCACTTGATTTTG-3′ (antisense). The PCR products were applied onto 2.0% (β-actin, EGFP,

and GAPDH) or 1.2% (Ago2) agarose gels and visualized under UV illumination after staining with ethidium bromide.

Western blotting. Anti-human Ago2 rabbit polyclonal antibody (Upstate, Lake Placid, NY), anti-actin rabbit polyclonal antibody (Sigma–Aldrich), anti-GAPDH mouse monoclonal antibody (GeneTex Inc., San Antonio, TX), peroxidase-conjugated anti-rabbit IgG polyclonal antibody (Santa Cruz Biotechnology, Santa Cruz, CA), and peroxidase-conjugated anti-mouse IgG polyclonal antibody (Santa Cruz Biotechnology) were purchased. The nucleotide sequences of siRNA for GAPDH (siGAPDH) with a 2-nucleotide overhang (underline) were 5′-CCAAAUAUGAUGACAUCAAGAAGGUAG-3′ (sense) and 5′-ACCUUCUUGAUGUCAUCAUAUUUGGAU-3′ (antisense). The sequences of siGAPDH correspond to the nucleotide region 791–815.

Cell extracts were prepared with lysis buffer composed of 10 mM Tris (pH 7.5), 0.1% SDS, 50 μg/ml aprotinin, 200 μM leupeptin, 2 mM PMSF, and 100 μM pepstatin A. Total protein concentration was measured by using a BCA Protein Assay Reagent Kit. The cell extract was subjected to 10 or 15% SDS–PAGE and transferred electrophoretically to a polyvi-

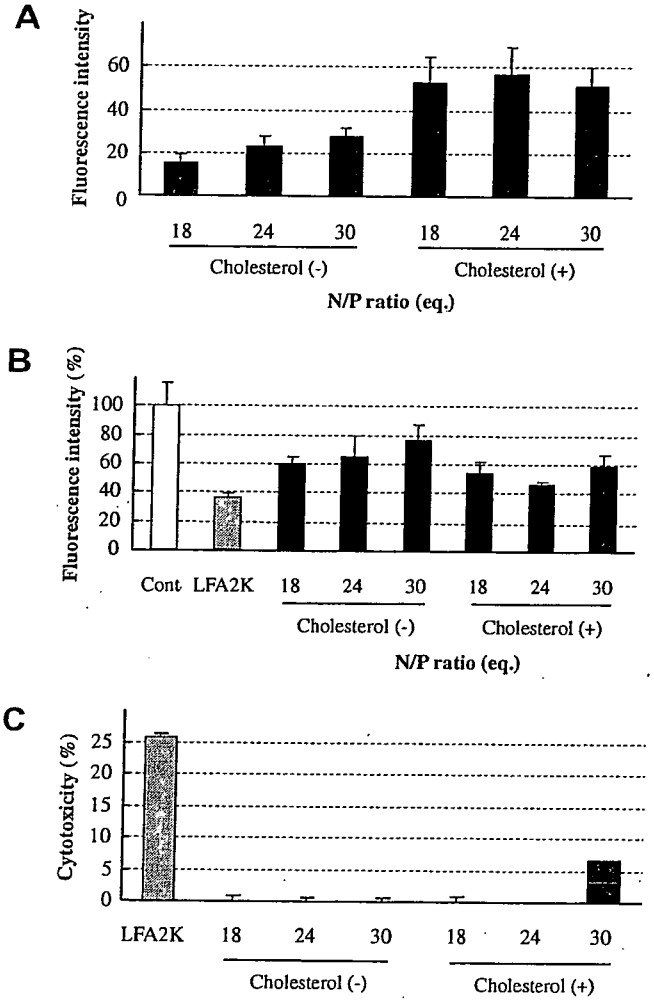

Fig. 1. Preparation of siRNA/PCLs complexes for siRNA transfection. (A) The amount of siRNA taken into HT1080 cells was determined after FAM-labeled siRNA/PCLs complexes had been allowed to interact with these cells for 4 h at 37 °C. PCLs with or without cholesterol were prepared and mixed with FAM-labeled siRNA at the various *N/P* ratios indicated in the figure. The fluorescence intensities of FAM in the cells were corrected for protein content. (B) RNAi efficiencies obtained by using PCLs were determined by conducting a quantitative gene silencing experiment. EGFP/HT-1080 cells were transfected with siEGFP complexed with PCLs (closed bar) or LFA2K (gray bar). The fluorescence intensity of EGFP was determined at 48 h post-transfection and corrected for protein content. The fluorescence intensity indicated as control (Cont, open bar) was that of cells not transfected with siRNA. Data represent the percent of control fluorescence intensity. (C) Cytotoxicity of PCLs against EGFP/HT1080 cells was determined. PCLs (closed bar) or LFA2K (gray bar) carrying siEGFP were allowed to interact with EGFP/HT1080 cells for 4 h at 37 °C and then removed. After further 24-h incubation, cell viability was estimated by conducting a modified MTT assay using Tetracolor ONE™. The percentage of damaged cells was calculated by setting non-treated cells as the control.

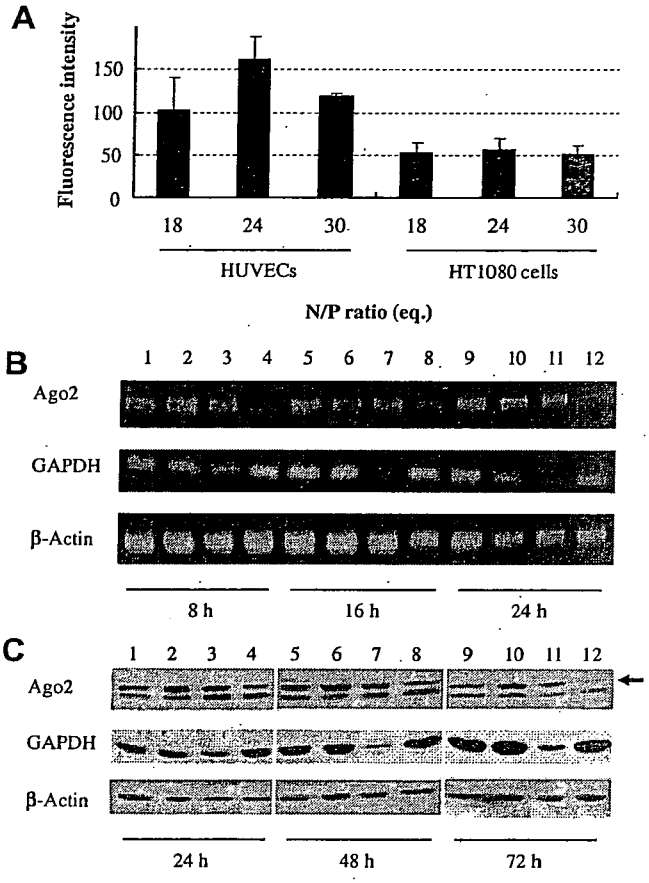

Fig. 2. Ago2 knockdown in HUVECs. (A) The amount of siRNA taken into HUVECs or HT1080 cells was determined after FAM-labeled siRNA/PCL complexes were allowed to interact with these cells for 4 h at 37 °C. PCLs composed of cetyl-PEI, DOPE, and cholesterol were prepared and mixed with FAM-labeled siRNA at the various *N/P* ratios indicated in the figure. The fluorescence intensities of FAM in the cells were corrected for protein content. (B) RT-PCR was performed by using HUVECs transfected with siAgo2 or siGAPDH. Total RNAs were isolated at 8, 16, and 24 h post-transfection, reverse transcribed, and applied to PCR using an Ago2, GAPDH or β-actin primer set. The PCR products were visualized by ethidium bromide under UV illumination. Lanes 1, 5, and 9, control without siRNA; lanes 2, 6, and 10, SiEGFP used as a non-silencing control; lanes 3, 7, and 11, SiGAPDH used as a control siRNA; and lanes 4, 8, and 12, SiAgo2. (C) Western blotting was performed by using HUVECs transfected with siAgo2 or siGAPDH. Cell extracts were prepared at 24, 48 or 72 h post-transfection. Ten micrograms of total protein was separated and incubated with anti-Ago2 rabbit polyclonal antibody, anti-actin rabbit polyclonal antibody or anti-GAPDH mouse monoclonal antibody. SiEGFP was used as non-silencing control; and siGAPDH, as control siRNA. Arrow shows the location of Ago2 protein. Lanes 1, 5, and 9, control without siRNA; lanes 2, 6, and 10, SiEGFP used as a non-silencing control; lanes 3, 7, and 11, SiGAPDH used as a control siRNA; and lanes 4, 8, and 12, SiAgo2.

nylidene difluoride (PVDF) membrane (MILLIPORE, Billerica, MA). After having been blocked for 1 h at room temperature with 5% skim milk in Tris–HCl-buffered saline containing 0.1% Tween 20 (TTBS, pH 7.4), the membrane was incubated with a primary antibody (β-actin and GAPDH; 0.1 μg/ml, Ago2; 2 μg/ml) for 2 h at room temperature. Then, it was incubated with a peroxidase-conjugated secondary antibody at a dilution of 1:10,000 for 1 h at room temperature. Each sample was developed by using a chemiluminescent substrate (ECL; Amersham Biosciences).

Cell growth assay. HUVECs were seeded onto 24-well plates at the density of 5×10^4 cells/dish and transfected with siAgo2 or siEGFP complexed with PCLs. After 0-, 24- or 48-h incubation, Tetracolor ONE™ was added to each well in accordance with the manufacturer's instructions. The amount of formazan formed in 2 h was measured by the microplate reader at a test wavelength of 492 nm and a reference wavelength of 630 nm.

Detection of apoptotic cells. HUVECs were seeded onto 35-mm dishes at the density of 2.5×10^5 cells/dish and transfected with siAgo2/ or siEGFP/PCL complexes. At 48 h after transfection, TUNEL staining was performed by using an ApopTag Plus Fluorescein In Situ Apoptosis Detection Kit (Chemicon International, Temecula, CA) according to the manufacturer's instructions. These cells were counterstained with DAPI and observed under an LSM510 META confocal Laser-Scanning-Microscope (Carl Zeiss, Oberkochen, Germany).

Tube formation assay. Matrigel (BD Biosciences Bedford, MA) was diluted to 4 mg/ml with EGM-2, added to 24-well plates, and allowed to undergo polymerization. HUVECs (5×10^5 cells/well) transfected with siAgo2 or siEGFP complexed with PCLs were then added to each well and incubated for 6 h at 37 °C. Photomicrographs were taken in 10 fields/group with an Olympus IMT-2 microscope (Olympus, Tokyo, Japan). The length of tubes was calculated by using software Image J (NIH, Bethesda, MD).

Results

Preparation of siRNA/PCLs complexes for siRNA delivery

At first, the adequate formulation of PCLs for siRNA transfection was determined by evaluating the uptake amount of siRNA, the knockdown efficiency, and the cytotoxicity. The sizes of siRNA/PCLs complexes prepared in this study were in the range of 130–155 nm, and the ξ-potentials of them were 30–50 mV. The uptake experiment showed that the presence of cholesterol in PCLs enhanced the uptake amount of FAM-labeled siAgo2 into HT1080 cells (Fig. 1A). In addition, the highest siRNA uptake was achieved when the *N*/*P* ratio of siRNA/PCLs complex was 24 equivalents (equiv). In the quantitative knockdown experiment, the siRNA formulation most taken up by HT1080 cells also showed the maximal knockdown efficiency (Fig. 1B). The cytotoxicity of siRNA/PCLs complexes was much lower than that of LFA2K (Fig. 1C).

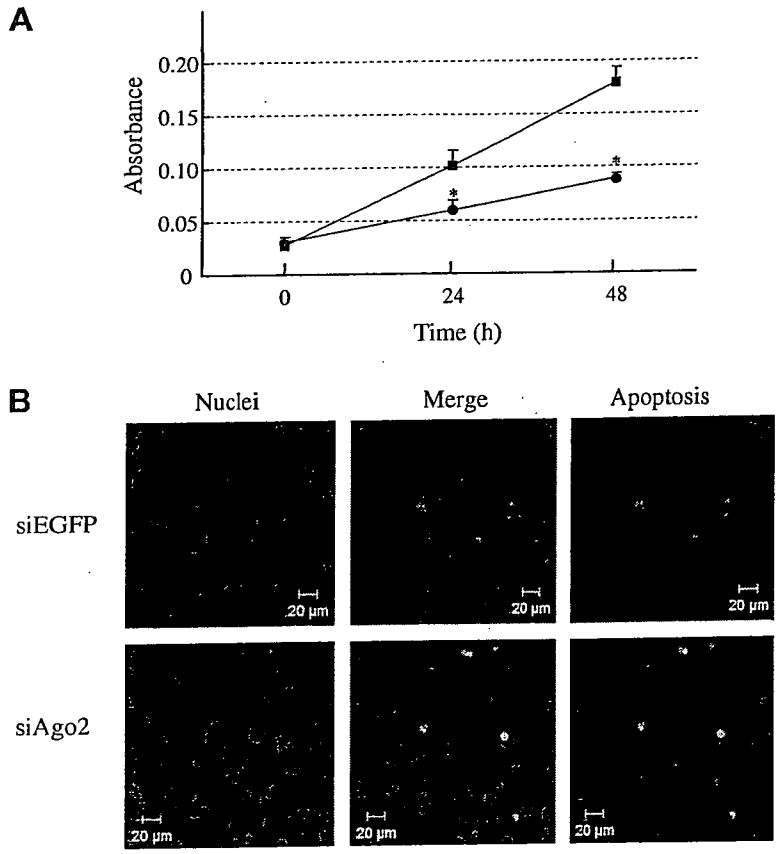

Fig. 3. Influence of Ago2 knockdown on the growth of HUVECs. (A) At 0, 24, and 48 h post-transfection, a modified MTT assay was performed with HUVECs transfected with siAgo2 (circles) or siEGFP (squares) complexed with PCLs. Data show the absorbance with SD bars. Significant differences from siEGFP group are indicated ($^*P < 0.01$). (B) Apoptosis of HUVECs transfected with siAgo2/PCL complexes was determined by TUNEL staining at 48 h post-transfection. The nuclei were counterstained with DAPI (blue). Apoptotic cells (FITC, green) were observed under an LSM510 META confocal Laser-Scanning-Microscope. Scale bars represent 20 μm.

Ago2 knockdown in HUVECs

To confirm Ago2 knockdown in HUVECs, these cells were transfected with siAgo2 (final concentration: 40 nM) complexed with PCLs. The uptake experiment indicated that the amount of FAM-labeled siAgo2 taken up was greater by HUVECs than by HT1080 cells (Fig. 2A). The optimal *N/P* ratio of siRNA/PCLs complexes for incorporating siRNA into HUVECs was 24 equiv, consistent with the result obtained for HT1080 cells. Based on these results from the formulation screening, we adopted the following formulation for use in subsequent experiments: cetyl-PEI/DOPE/cholesterol = 0.05/1/0.5 as a molar ratio, *N/P* ratio = 24 equiv. The RT-PCR data showed that siAgo2 down-regulated the expression of Ago2 mRNAs in HUVECs (Fig. 2B). The specificity of Ago2 knockdown was confirmed by the transfection with siEGFP or siGAPDH. Neither siEGFP nor siGAPDH affected the expression of Ago2 mRNA, and siGAPDH suppressed the expression of GAPDH mRNA. These data indicate that the knockdown of Ago2 occurred in a siAgo2-dependent manner. The Western blotting data demonstrated that the expression of Ago2 protein was actually diminished by siAgo2 transfection (Fig. 2C).

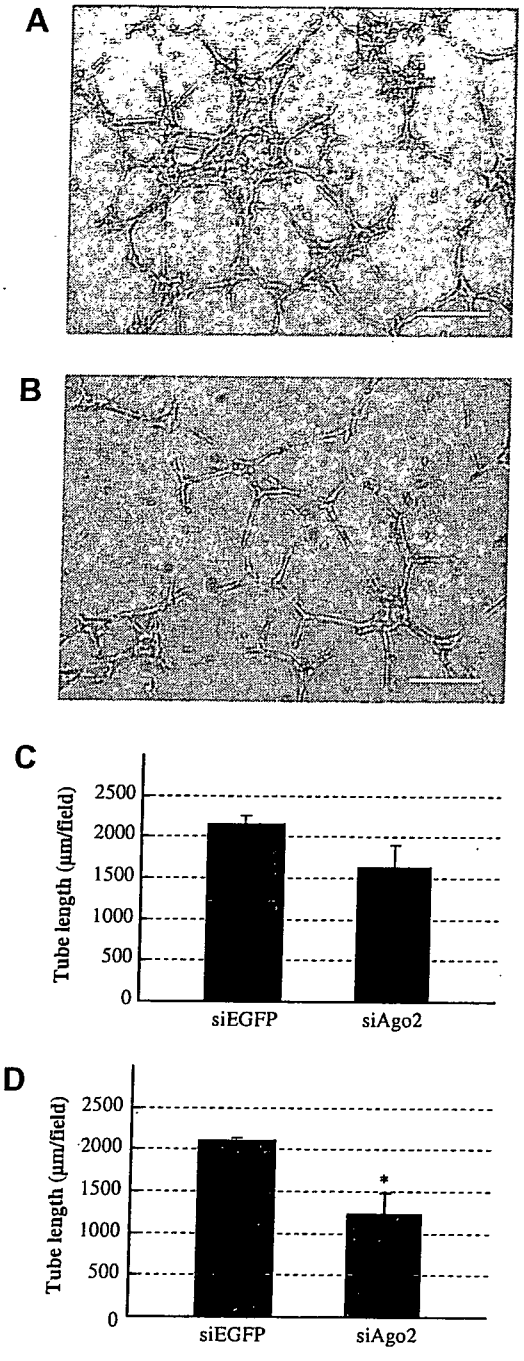

Fig. 4. Inhibition of tube formation by Argonaute2 knockdown. Tube formation assay was performed with HUVECs transfected with siAgo2/PCL complexes. The transfected cells were collected at 24 (C) or 48 h (A, B, and D) post-transfection and incubated on Matrigel for 6 h at 37 °C in 5% CO_2. (A, B) Photomicrographs show the tube formation of HUVECs transfected with siEGFP (A) or siAgo2 (B). Scale bars represent 20 μm. (C and D) The length of tubes was calculated by using the software Image J. Significant difference from siEGFP group is indicated ($^*P < 0.05$).

Influence of Ago2 knockdown on angiogenic potentials of HUVECs

To investigate the influence of Ago2 knockdown on the properties of endothelial cells, HUVECs were transfected with siAgo2/PCL complexes. The influence of Ago2 knockdown on the proliferation of HUVECs was determined by using a modified MTT assay. As shown in Fig. 3A, the treatment with siAgo2 significantly suppressed the growth of HUVECs in comparison to that with siEGFP, a control siRNA ($P < 0.001$). TUNEL staining showed that a certain population of HUVECs treated with siAgo2 underwent apoptosis at 48 h after the transfection (Fig. 3B). The percentage of apoptotic cells was about 20% in siAgo2-treated HUVECs. This result indicates that the growth inhibition by Ago2 knockdown was partially caused by the induction of apoptosis. On the other hand, Ago2 knockdown did not induce apoptosis of HT1080 cells in the similar experiment (Supplementary Fig. 1).

In the tube formation assay, the HUVECs transfected with siEGFP formed capillary-like structures (Fig. 4A). In contrast, the treatment with siAgo2 suppressed the tube formation of HUVECs (Fig. 4B). The length of tubes, an indicator of tube formation, was significantly reduced by the knockdown of Ago2 when HUVECs were used for this assay at 48 h post-transfection (Fig. 4C and D). These results indicate that siAgo2 inhibited indispensable events of angiogenesis.

Discussion

In the present study, we demonstrated that the knockdown of Ago2 resulted in the loss of the angiogenic potential of HUVECs, thus suggesting that Ago2 is required for angiogenesis. We consider one of the reasons to be indirect effects related to the miRNA system. The knockdown of Ago2 could affect the expression levels of some critical miRNAs required for the formation of angiogenic vessels.

For instance, it was reported that miR-221 and miR222 control the ability of HUVECs to form new capillaries [12]. However, the knockdown of Ago2 is considered to affect most miRNAs not just miR-221/2. As well as the knockdown of Ago2, the deletion of Dicer function resulted in failure of mouse embryonic angiogenesis [13]. These results indicate that the miRNA system is indispensable for angiogenesis, in which Ago2 also plays a critical role.

Angiogenesis is a crucial event for many severe diseases such as cancer. Therefore, the development of antiangiogenic RNAi therapy have been widely investigated [3]. The knockdown of angiogenic factor such as vascular endothelial growth factor is expected to be a novel therapeutic strategy [3]. Our data suggest that Ago2 might be a unique therapeutic target for antiangiogenic RNAi therapy. Since siAgo2 not only cleaves the mRNA of Ago2 but also occupies the protein of Ago2 that is required for RNAi, the use of siAgo2 is considered to be an efficient strategy to disturb an ordered miRNA system. The amount of Ago2 protein would not be rate determining in this strategy, whereas other siRNA requires sufficient Ago2 protein. Therefore, the knockdown of Ago2 is a unique approach for inhibiting angiogenesis. However, a siRNA delivery system that targets endothelial cells specifically is necessary to apply siAgo2 for antiangiogenic therapy, since siAgo2 would be expected to affect the entire miRNA system.

In the present study, we determined the optimal formulation of PCLs by determining the gene silencing efficiency and cytotoxicity and demonstrated PCLs to be a novel siRNA vector. PCLs carrying siAgo2 attenuated the angiogenic potential of HUVECs. In the case that PCLs carrying siAgo2 are applied *in vivo*, the availability of them will be extended by surface modification of the liposomes with functional molecules such as polyethyleneglycol and certain ligands targeting angiogenic endothelial cells. In our previous study, we demonstrated that Ala-Pro-Arg-Pro-Gly (APRPG) is a useful peptide for the active targeting of angiogenic vessels [17]. APRPG-modified liposomal doxorubicin actually caused effective tumor growth suppression through damaging angiogenic endothelial cells [17]. APRPG-modified liposomal siAgo2 might thus be a good candidate for use in antiangiogenic RNAi therapy.

Acknowledgments

This research was supported by Research on Advanced Medical Technology on Health and Labour Sciences Research Grants, Ministry of Health, Labour and Welfare, Japan.

Appendix A. Supplementary data

Supplementary data associated with this article can be found, in the online version, at doi:10.1016/j.bbrc.2008.01.074.

References

[1] A. Fire, S. Xu, M.K. Montgomery, S.A. Kostas, S.E. Driver, C.C. Mello, Potent and specific genetic interference by double-stranded RNA in *Caenorhabditis elegans*, Nature 391 (1998) 806–811.
[2] S.M. Elbashir, J. Harborth, W. Lendeckel, A. Yalcin, K. Weber, T. Tuschl, Duplexes of 21-nucleotide RNAs mediate RNA interference in cultured mammalian cells, Nature 411 (2001) 494–498.
[3] S.I. Pai, Y.Y. Lin, B. Macaes, A. Meneshian, C.F. Hung, T.C. Wu, Prospects of RNA interference therapy for cancer, Gene Ther. 13 (2006) 464–477.
[4] R.I. Gregory, T.P. Chendrimada, N. Cooch, R. Shiekhattar, Human RISC couples microRNA biogenesis and posttranscriptional gene silencing, Cell 123 (2005) 631–640.
[5] K. Okamura, A. Ishizuka, H. Siomi, M.C. Siomi, Distinct roles for Argonaute proteins in small RNA-directed RNA cleavage pathways, Genes Dev. 18 (2004) 1655–1666.
[6] J. Liu, M.A. Carmell, F.V. Rivas, C.G. Marsden, J.M. Thomson, J.J. Song, S.M. Hammond, L. Joshua-Tor, G.J. Hannon, Argonaute2 is the catalytic engine of mammalian RNAi, Science 305 (2004) 1437–1441.
[7] G. Meister, M. Landthaler, A. Patkaniowska, Y. Dorsett, G. Teng, T. Tuschl, Human Argonaute2 mediates RNA cleavage targeted by miRNAs and siRNAs, Mol. Cell 15 (2004) 185–197.
[8] C. Matranga, Y. Tomari, C. Shin, D.P. Bartel, P.D. Zamore, Passenger-strand cleavage facilitates assembly of siRNA into Ago2-containing RNAi enzyme complexes, Cell 123 (2005) 607–620.
[9] M. Cristofanilli, C. Charnsangavej, G.N. Hortobagyi, Angiogenesis modulation in cancer research: novel clinical approaches, Nat. Rev. Drug Discov. 1 (2002) 415–426.
[10] K. Shimizu, T. Asai, N. Oku, Antineovascular therapy, a novel antiangiogenic approach, Expert Opin. Ther. Targets 9 (2005) 63–76.
[11] N. Ferrara, K.J. Hillan, W. Novotny, Bevacizumab (Avastin), a humanized anti-VEGF monoclonal antibody for cancer therapy, Biochem. Biophys. Res. Commun. 333 (2005) 328–335.
[12] L. Poliseno, A. Tuccoli, L. Mariani, M. Evangelista, L. Citti, K. Woods, A. Mercatanti, S. Hammond, G. Rainaldi, MicroRNAs modulate the angiogenic properties of HUVECs, Blood 108 (2006) 3068–3071.
[13] W.J. Yang, D.D. Yang, S. Na, G.E. Sandusky, Q. Zhang, G. Zhao, Dicer is required for embryonic angiogenesis during mouse development, J. Biol. Chem. 280 (2005) 9330–9335.
[14] R.C. Ryther, A.S. Flynt, J.A. Phillips 3rd, J.G. Patton, siRNA therapeutics: big potential from small RNAs, Gene Ther. 12 (2005) 5–11.
[15] N. Oku, Y. Yamazaki, M. Matsuura, M. Sugiyama, M. Hasegawa, M. Nango, A novel non-viral gene transfer system, polycation liposomes, Adv. Drug Deliv. Rev. 52 (2001) 209–218.
[16] S. Yamakawa, Y. Furuyama, N. Oku, Development of a simple cell invasion assay system, Biol. Pharm. Bull. 23 (2000) 1264–1266.
[17] N. Oku, T. Asai, K. Watanabe, K. Kuromi, M. Nagatsuka, K. Kurohane, H. Kikkawa, K. Ogino, M. Tanaka, D. Ishikawa, H. Tsukada, M. Momose, J. Nakayama, T. Taki, Anti-neovascular therapy using novel peptides homing to angiogenic vessels, Oncogene 21 (2002) 2662–2669.

Available online at www.sciencedirect.com
ScienceDirect
International Journal of Pharmaceutics 353 (2008) 65–73
INTERNATIONAL JOURNAL OF PHARMACEUTICS
www.elsevier.com/locate/ijpharm

A metronomic schedule of cyclophosphamide combined with PEGylated liposomal doxorubicin has a highly antitumor effect in an experimental pulmonary metastatic mouse model

Emi Shiraga [a], Jose Mario Barichello [a,b], Tatsuhiro Ishida [a,*], Hiroshi Kiwada [a]

[a] *Department of Pharmacokinetics and Biopharmaceutics, Subdivision of Biopharmaceutical Science, Institute of Health Biosciences, The University of Tokushima, 1-78-1 Sho-machi, Tokushima 770-8505, Japan*
[b] *Japan Association for the Advancement of Medical Equipment, Tokyo 113-0033, Japan*

Received 10 August 2007; received in revised form 11 October 2007; accepted 10 November 2007
Available online 17 November 2007

Abstract

Metronomic chemotherapy is a novel approach to the control of advanced cancer, as it appears to preferentially inhibit endothelial cell activity in the growing vasculature of tumors. Doxorubicin-containing sterically stabilized liposomes (DXR-SL) accumulate in large amounts in tumor tissue, resulting in enhanced antitumor effects of the encapsulated DXR. In the present study, it was hypothesized that metronomic chemotherapy may further augment the accumulation of DXR-SL, improving its therapeutic efficacy. This study tests the antitumor efficacy for the combination of a metronomic cyclophosphamide (CPA)-dosing schedule with sequential intravenous injections of DXR-SL in the treatment of lung metastatic B16BL6 melanoma-bearing mice. Three dosing schedules for the combination of metronomic CPA injections (s.c. 170 mg/kg every 6 days) plus either a low or a high dose of DXR-SL (i.v. 1 or 5 mg/kg every 6 days) were set: Schedule I, DXR-SL was given 3 days before the first CPA treatment; Schedule II, DXR-SL and CPA were given simultaneously; and, Schedule III, DXR-SL was given 3 days after the first CPA treatment. Lung weight and median survival time (MST) were evaluated. As expected, both the dosing schedule as well as the dose of DXR-SL improved therapeutic efficacy. Schedule I with the low DXR dose and Schedule II with the low or high DXR dose significantly increased MST, compared with regular metronomic CPA therapy. Under the dosing schedules (Schedule I with the low DXR dose and Schedule II with the high DXR), there was a strong relationship between increased MST and decreased lung weight. However, Schedule I with high DXR dose resulted in significantly lower lung weights, but did not increase MST, suggesting that chemotherapy may result in increased toxicity in some conditions. Although treatment regimens require optimization, the results of the present study may prove useful in further explorations of combining metronomic chemotherapy with liposomal anticancer drugs in the treatment of solid tumors.

Keywords: Combination therapy; Metronomic chemotherapy; Liposomal anticancer drug; PEGylated liposome; Cyclophosphamide; Doxorubicin

1. Introduction

Traditionally, systemic anti-cancer therapy has been dominated by the use of cytotoxic chemotherapeutics, which often are administered as a single dose or in short courses of therapy using the maximum tolerated dose (MTD) (conventional chemotherapy). MTD chemotherapy requires prolonged breaks between successive cycles of therapy due to toxicity (Kerbel and Kamen, 2004). On the other hand, a novel chemotherapeutic regimen, metronomic chemotherapy, recently has been advocated (Kerbel and Kamen, 2004; Gille et al., 2005; Munoz et al., 2005; Laquente et al., 2007; Tonini et al., 2007). Metronomic chemotherapy refers to the frequent administration of

Abbreviations: CHOL, cholesterol; CPA, cyclophosphamide; DXR, doxorubicin; DXR-SL, DXR-containing PEGylated liposomes; EPR, enhanced permeability and retention; HEPC, hydrogenated egg phosphatidylcholine; MPS, mononuclear phagocyte system; $mPEG_{2000}$-DSPE, 1,2-distearoyl-*sn*-glycero-3-phosphoethanolamine-*n*-[methoxy (polyethylene glycol)-2000]; MST, median survival time; MTD, maximum tolerated dose; PEG, polyethylene glycol; TβR-I, transforming growth factor type I receptor; TSP-1, thrombospondin-1; WBC, white blood cells.

* Corresponding author. Tel.: +81 88 633 7260; fax: +81 88 633 7260.
E-mail address: ishida@ph.tokushima-u.ac.jp (T. Ishida).

0378-5173/$ – see front matter © 2007 Elsevier B.V. All rights reserved.
doi:10.1016/j.ijpharm.2007.11.020

chemotherapeutics at doses significantly below the MTD without prolonged drug-free breaks. The therapy shows lower toxicity, allowing prolonged treatment.

The target of metronomic chemotherapy is believed to be the genetically stable endothelial cells within the vascular bed of the tumor, rather than tumor cells with a high rate of mutations (Browder et al., 2000). Thus, this strategy is categorized as an anti-angiogenic chemotherapy (Browder et al., 2000; Kerbel and Kamen, 2004; Munoz et al., 2005; Laquente et al., 2007; Tonini et al., 2007). Various chemotherapeutics, such as cyclophosphamide (CPA), vinblastine, methotrexate, etoposide and tegafur, are used for metronomic chemotherapy (Klement et al., 2000, 2002; Bello et al., 2001; Shaked et al., 2005; Klink et al., 2006; Munoz et al., 2006); among these, CPA is most frequently used. CPA is traditionally used for chemotherapy as an alkylating agent, which kills the tumor cells directly. However, it is reported that at lower doses, CPA enhances expression of thrombospondin-1 (TSP-1) in stromal and tumor cells (Hamano et al., 2004). TSP-1, a component of the extracellular matrix, which is secreted and found in circulation, is a well-known endogenous inhibitor of angiogenesis (de Fraipont et al., 2001; Lawler, 2002). The molecule primarily binds to CD36 receptors, which are expressed by endothelial cells of tumors (Dawson et al., 1997). It is thought that this interaction blocks proliferation and induces apoptosis in tumor endothelial cells, thereby inducing collapse of angiogenic vessels (Dawson et al., 1997; Guo et al., 1997; Jimenez et al., 2000). Consequently, metronomic CPA-dosing reduces tumor neovascularization, thus suppressing tumor growths (Browder et al., 2000; Kerbel and Kamen, 2004).

Chemotherapy delivered in nanocarriers has been developed to improve the clinical treatment of solid tumors by achieving high accumulation of chemotherapeutic agents in tumor tissues but limited accumulation in healthy organs. Doxil, doxorubicin-containing sterically stabilized (PEGylated) liposomes, is one such drug that has already been used clinically (Grunaug et al., 1998; Safra et al., 2000; Krown et al., 2004). It is well-known that sterically stabilized (PEGylated) liposomes (SL) show prolonged circulating times as a result of reduced opsonization by serum proteins and lowered recognition by cells of the mononuclear phagocyte system (MPS) (Lasic et al., 1991; Torchilin et al., 1994). Consequently, SL accumulate in solid tumors via angiogenic blood vessels that have increased permeability (Jain, 1987; Papahadjopoulos et al., 1991; Wu et al., 1993; Yuan et al., 1995; Forssen et al., 1996; Vaage et al., 1997), due to the so-called "enhanced permeability and retention (EPR) effect" (Maeda et al., 2000). As described above, metronomic injection of low-dose CPA induces the collapse of tumor angiogenic vessels. This may enhance the EPR effect for SL, resulting in increased nanocarrier accumulation in tumor tissue. The use of metronomic CPA chemotherapy combined with DXR-SL may thus have clinical significance and practical importance in treating solid tumors.

Therefore, the objective of the present study was to determine whether the combination of metronomic cyclophosphamide (CPA)-administration and sequential intravenous injections of DXR-SL improves antitumor efficacy in lung metastatic B16BL6 melanoma-bearing mice. The results indicated that a combination approach may improve therapeutic efficacy under some dosage regimens, although this approach is accompanied by an increase in toxicity.

2. Materials and methods

2.1. Materials

Hydrogenated egg phosphatidylcholine (HEPC) and 1,2-distearoyl-*sn*-glycero-3-phosphoethanolamine-*n*-[methoxy (polyethylene glycol)-2000] ($mPEG_{2000}$-DSPE) were generously donated by Nippon Oil and Fat (Tokyo, Japan). Doxorubicin (DXR) was generously donated by Daiichi Pharmaceutical. (Tokyo, Japan). Cholesterol (CHOL) and cyclophosphamide (CPA) were purchased from Wako Pure Chemical (Osaka, Japan). FITC-labeled rabbit anti-rat IgG heavy and light chain polyclonal antibody was purchased from Abcam (Cambridge, UK). Rat monoclonal anti-mouse CD45 antibody was purchased from R&D systems (CA, USA). All other reagents were of analytical grade.

2.2. Animal and tumor cell line

Male C57BL/6 mice, 5 weeks old, were purchased from Japan SLC (Shizuoka, Japan). The experimental animals were allowed free access to water and mouse chow, and were housed under controlled environmental conditions (constant temperature, humidity, and 12 h dark–light cycle). All animal experiments were evaluated and approved by the Animal and Ethics Review Committee of the University of Tokushima.

The pulmonary metastatic mouse melanoma cell line, B16BL6, was maintained in DMEM (Wako Pure Chemical) supplemented with 10% heat-inactivated FBS (Japan Bioserum, Hiroshima, Japan), 10 mM L-glutamine, 100 units/ml penicillin and 100 μg/ml streptomycin in a 5% CO_2 air incubator at 37 °C.

2.3. Preparation of liposomes

PEGylated liposomes (sterically stabilized liposomes, SL) were composed of HEPC/CHOL/$mPEG_{2000}$-DSPE (2/1/0.1 molar ratio). Liposomes were prepared using the thin-film hydration technique (Ishida et al., 2003). Briefly, the lipids were dissolved in chloroform and, after evaporation of the organic solvent, the resulting lipid film was hydrated with 250 mM ammonium sulfate solution (pH 5.5). The liposomes were sized by subsequent extrusion through polycarbonate membrane filters (Nuclepore, CA, USA) with pore sizes of 400, 200, and 100 nm. The mean diameter of the liposomes was approximately 100 nm, as determined using a NICOMP 370 HPL submicron particle analyzer (Particle Sizing System, CA, USA). The phospholipid concentration was determined by colorimetric assay (Bartlett, 1959). DXR was encapsulated into the liposomes by remote loading using an ammonium sulfate gradient, as previously described (Bolotin et al., 1994). Following extrusion, the external buffer was exchanged by eluting through a Sephadex G-50 column equilibrated with 10% sucrose. DXR was dissolved in a sucrose solution at a concentration of 10 mg/ml.

The DXR solution then was added to the liposome solution at a concentration of 0.2 mg DXR/1 mg phospholipid. The mixture was incubated in a 65 °C water bath for 1 h with slow agitation. After loading DXR into the liposomes, unencapsulated DXR was removed using a Sephadex G-50 column in HEPES buffered saline (25 mM HEPES, 140 mM NaCl, pH 7.4). DXR-loading efficiency was >90%.

2.4. In vivo assessment of tumor growth

B16BL6 cells were grown to 80–90% confluence in a 10 cm culture dish, harvested, and resuspended in cold PBS (51 mM Na_2HPO_4, 12 mM NaH_2PO_4, 77 mM NaCl, pH 7.4). The cells (5×10^4) in 0.2 ml PBS were inoculated into the tail vein of C57BL/6 mice.

CPA and DXR treatments were started 14 days after inoculating the mice with B16BL6 cells, because our earlier study demonstrated that extensive progression of tumor nodules on the surface of the lungs was evident 14 days post-inoculation (Li et al., 2005). The antitumor effect of the treatments was evaluated by survival time and lung weight at time of death. Body weight also was evaluated as a surrogate marker of toxicity.

2.5. CPA and DXR-SL dosing schedules

The CPA and DXR-SL treatments were as follows:

(1) *Conventional dosing of CPA*. Mice ($n=5$) received two cycles of CPA treatment separated by a 3-week interval. Each cycle consisted of a total of three doses of CPA (150 mg/kg per dose) administered subcutaneously every other day (total dose of 450 mg/kg, i.e., MTD, maximum tolerated dose) (Browder et al., 2000).
(2) *Metronomic dosing of CPA*. Mice received eight doses of CPA (170 mg/kg per dose) administered subcutaneously at 6-day intervals (Browder et al., 2000).
(3) *Conventional dosing of DXR-SL*. Mice received DXR-SL (1 or 5 mg/kg) intravenously at 6-day intervals until the mice died.
(4) *Combination dosing of CPA with DXR-SL*:
   (i) *Schedule I (low or high dose of DXR-SL)*. CPA (170 mg/kg) was administered subcutaneously at 6-day intervals. Three days *before* CPA injection (11 day after tumor inoculation), high (5 mg/kg) and low (1 mg/kg) dose DXR-SL administered intravenously at 6-day intervals.
   (ii) *Schedule II (low or high dose of DXR-SL)*. CPA (170 mg/kg) was administered subcutaneously and high (5 mg/kg) or low (1 mg/kg) dose DXR-SL intravenously at 6-day intervals. The treatment was started at day 14 after tumor inoculation.
   (iii) *Schedule III (low or high dose of DXR-SL)*. CPA (170 mg/kg) was administered subcutaneously at 6-day intervals. Three days *after* the first CPA injection (17 day after tumor inoculation), high (5 mg/kg) or low (1 mg/kg) DXR-SL was administered intravenously and the injections were continued at 6-day intervals.

2.6. Toxicity assessment

To avoid the influence of tumorigenesis on toxicity assessment, normal C57BL/6 mice were used. Mice received six cycles of CPA or DXR-SL treatment administered at 6-day intervals. One cycle consisted of either subcutaneous administration of CPA (170 mg/kg) or intravenous injection of DXR-SL (1 or 5 mg/kg). After treatment was initiated, body weight was measured every 3 days. To determine change in the number of circulating white blood cells (WBC), blood was collected via retro-orbital puncture 7, 19 and 31 days after treatment was begun. Blood samples were washed twice with cold PBS and blood cells were collected by centrifugation for 5 min at 2000 rpm and 4 °C. Blood cells were blocked with 1% BSA/PBS for 15 min at room temperature and then were incubated with primary antibody (rat monoclonal anti-mouse CD45 antibody) for 30 min. After washing with cold PBS, samples were incubated for an additional 30 min with secondary antibody (FITC-labeled rabbit anti-rat IgG heavy- and light-chain polyclonal antibody). WBC number was determined using flow cytometry (Guava EasyCyte Mini System, GE Healthcare, CA, USA).

2.7. Statistics

All values are expressed as the mean ± S.D. Statistical analysis was performed with a two-tailed unpaired t-test using GraphPad InStat software (GraphPad Software, CA, USA). The level of significance was set at $p < 0.05$.

3. Results

3.1. Antitumor effect of a metronomic CPA-dosing schedule on pulmonary metastatic B16BL6 melanoma-bearing mice

The pulmonary metastatic B16BL6 melanoma bearing mouse model was employed in the present study because the antitumor effects of metronomic CPA chemotherapy have not yet been reported for a plumonary metastatic model. Conventional and metronomic CPA-dosing schedules significantly improved median survival time (MST) of tumor-bearing mice compared with controls (no-treatment). In addition, the metronomic schedule remarkably prolonged MST compared with the conventional schedule (control = 24.0 days, conventional schedule = 36.5 days and metronomic schedule = 50.0 days) (Fig. 1A). In experimental pulmonary metastasis models, lung weight reflects the growth of pulmonary metastases (Fig. 1B). Conventional and metronomic CPA-dosing schedules significantly inhibited the growth of cells that had metastasized to the lungs compared with control (no-treatment). Moreover, the metronomic schedule was significantly more efficient than the conventional schedule (Fig. 1B). Throughout these experiments, animals did not exhibit significant weight loss (data not shown). These results confirmed that the metronomic CPA-dosing schedule is more effective than the conventional dosing schedule with no severe side effects in lung metastatic B16BL6 melanoma-bearing mice. In contrast, when the dosing was started 3 days after B16BL6 cell-inoculation, lung weights

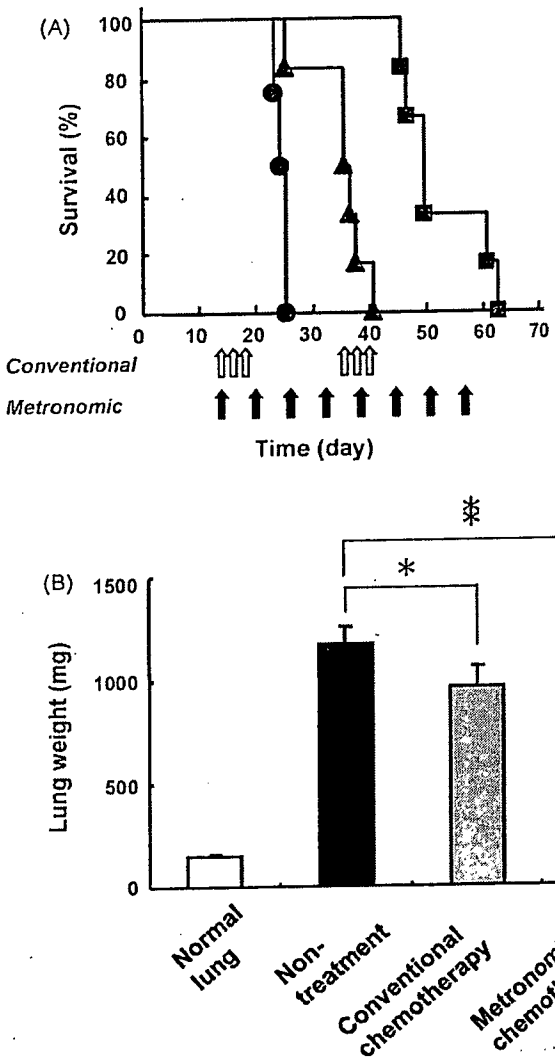

Fig. 1. Effect of either conventional (maximum tolerated dose) or metronomic CPA-dosing on (A) survival of B16BL6-bearing mice and (B) lung weight at time of death. Control (no treatment (●), conventional dosing (▲), 2 cycles consisting of 3 doses (white arrows) of 150 mg/kg administered every other day (total 450 mg/kg) with 3 weeks between cycles. Metronomic dosing (■), 8 doses of 170 mg/kg (black arrows) administered at 6-day intervals. $N=5$ mice per group. $^{*}p<0.05$; $^{**}p<0.005$ vs. control.

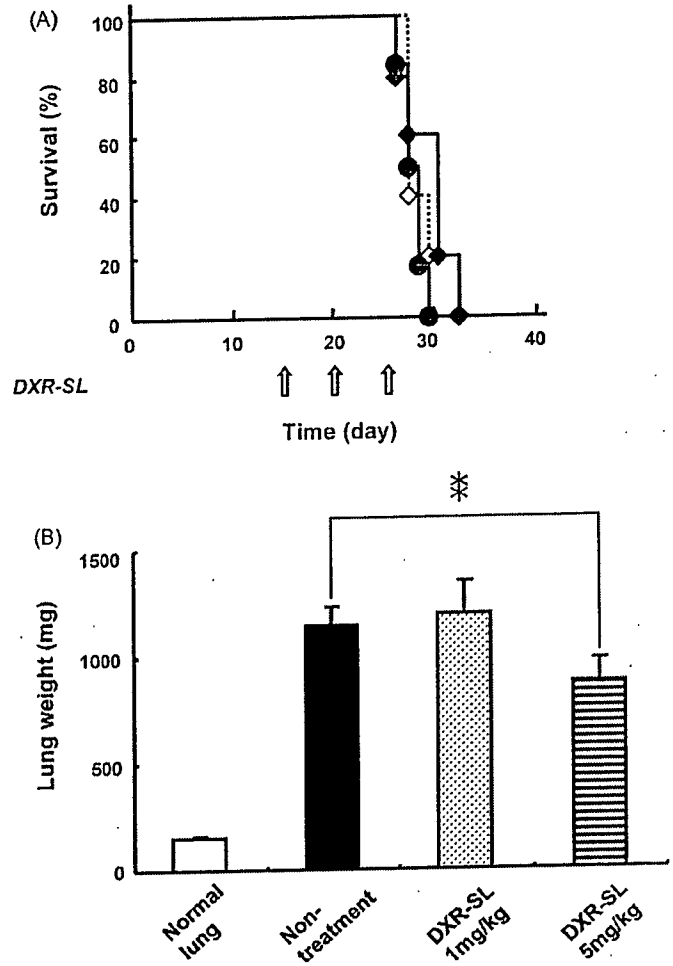

Fig. 2. Effect of DXR-SL (high or low dose) on (A) survival of B16BL6-bearing mice and (B) lung weight at time of death. Control (●). DXR-SL (◇ with dotted line), 3 doses of 1 mg/kg administered at 6-day intervals. DXR-SL (◆), 3 doses of 5 mg/kg administered at 6-day intervals. $N=5$ mice per group. $^{**}p<0.005$ vs. control.

did not increase, regardless of which CPA-dosing schedule was used. No tumor nodules were evident on the surface of lungs (data not shown). Thus, when the growth and formation of pulmonary metastases were minimal, because only 3 days had passed since inoculation with melanoma cells, both schedules had remarkable therapeutic efficiency in this animal model.

3.2. Antitumor effect of sequential DXR-SL administration on pulmonary metastatic B16BL6 melanoma bearing mice

Two different doses of DXR-SL (low and high) were administered intravenously every 6 days, 3 cycles, into tumor bearing mice from 14 day after tumor cells-inoculation. No significant increases in the MST were observed for either DXR-SL dose when administered according to a conventional dosing schedule (Fig. 2A): MSTs of control (no-treatment), low and high DXR-SL doses were 28.4, 29.0 and 32.0 days, respectively. However, lung weights of tumor-bearing mice indicated that the higher DXR-SL dose slightly inhibited the growth of metastasized cells (Fig. 2B). These findings demonstrate that sequential administration of DXR-SL had a very mild antitumor effect, although the effect did not appear to be related to extension of survival time in tumor-bearing mice. Throughout this experiment, no significant weight loss was observed (data not shown).

3.3. Antitumor effect of the combination of a metronomic CPA-dosing schedule and sequential administration of DXR-SL

To examine the effect of the combination therapy, CPA was metronomically administered either alone or plus DXR-SL (low or high dose). Sequential administration of DXR-SL (every 6 days) was started either 3 days before (Schedule I), on the same day as (Schedule II), or 3 days after (Schedule III), the first CPA injection because the metronomic CPA-dosing schedule may have affected the accumulation of SL in tumor tissue by increasing the permeability of angiogenic blood vessels. Schedules I, II

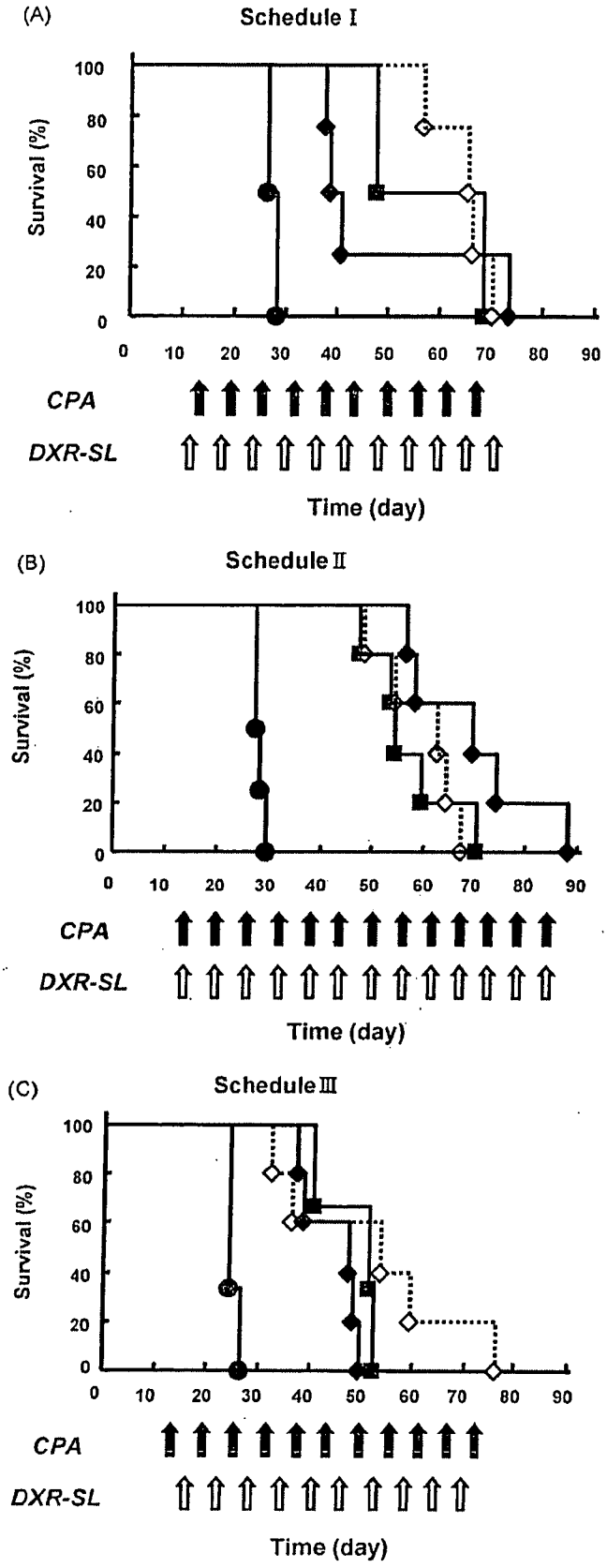

Fig. 3. Effect of the combination of metronomic CPA- and sequential DXR-SL-dosing on survival of B16BL6-bearing mice. (A) Schedule I (low or high dose of DXR-SL): CPA (170 mg/kg) was administered subcutaneously at 6-day intervals. Three days *before* CPA injection (11 days after tumor inoculation), high (5 mg/kg) or low (1 mg/kg) DXR-SL was administered intravenously at 6-day intervals. (B) Schedule II (low or high dose of DXR-SL): CPA (170 mg/kg) was administered subcutaneously and high (5 mg/kg) or low (1 mg/kg) DXR-SL intravenously at 6-day intervals (14 days after tumor inoculation). (C) Schedule III (low or high dose of DXR-SL): CPA (170 mg/kg) was administered subcutaneously at 6-day intervals. Three days *after* the first CPA injection (17 day after tumor inoculation), high (5 mg/kg) or low (1 mg/kg) dose DXR-SL was administered intravenously and the injections were continued at 6-day intervals. Control (●). Metronomic schedule (■), 170 mg/kg administered at 6-day intervals. Combination of metronomic CPA-dosing (170 mg/kg, thin black arrows) and low dose DXR-SL (1 mg/kg, thin gray arrows) (◊ with dotted line). Metronomic CPA-dosing schedule (170 mg/kg, thin black arrows) and high dose DXR-SL (5 mg/kg, thin gray arrows) (♦).

Table 1
Median survival time for each treatment schedule group

	Median survival time (day)			
	None	Schedule I	Schedule II	Schedule III
Control		28.0		
Metronomic dosing		52.0		
CPA (170 mg/kg) + DXR-SL (high, 5 mg/kg)	–	40.5	69.00	51.0
CPA (170 mg/kg) + DXR-SL (low, 1 mg/kg)	–	66.5	63.0	54.0

The results were calculated on the basis of the data presented in Fig. 3.

and III (described in detail in Section 2) were tested in pulmonary metastatic B16BL6 melanoma bearing mice. All MSTs are summarized in Table 1. The combination of a metronomic schedule of CPA with DXR-SL prolonged MST compared to control (non-treatment) (Fig. 3). For Schedule I, only the combination of CPA with the *high* dose of DXR-SL prolonged MST compared with the metronomic schedule of CPA (Fig. 3A, Table 1). In contrast, for Schedule II, the combination of CPA with either the *low* or *high* dose of DXR-SL prolonged MST compared with the metronomic CPA-dosing schedule (Fig. 3B, Table 1). Interestingly, for Schedule III, the combination of CPA with DXR-SL did not prolong, but rather shortened, MST compared with the metronomic CPA-dosing schedule (Fig. 3C, Table 1). The results shown in Fig. 4 indicate that the combined therapy significantly inhibited the growth cells that had metastasized in the lung compared to control (no-treatment). The Schedule I combined therapy significantly inhibited growth of metastasized cells, compared with the metronomic CPA-dosing schedule, regardless of the dose of DXR-SL (Fig. 4A). The Schedule II combined therapy with the high dose of DXR-SL significantly inhibited growth of metastasized cells, while the low dose of DXR-SL did not (Fig. 4B). The Schedule III combined therapy did not induce any significant inhibition of metastatic cell growth (Fig. 4C).

3.4. Toxicity of the combination of the metronomic CPA-dosing schedule and sequential administration of DXR-SL

Because the presence of a tumor influences bone marrow function and because treatment of tumor-bearing mice with chemotherapeutic agents makes data interpretation extremely

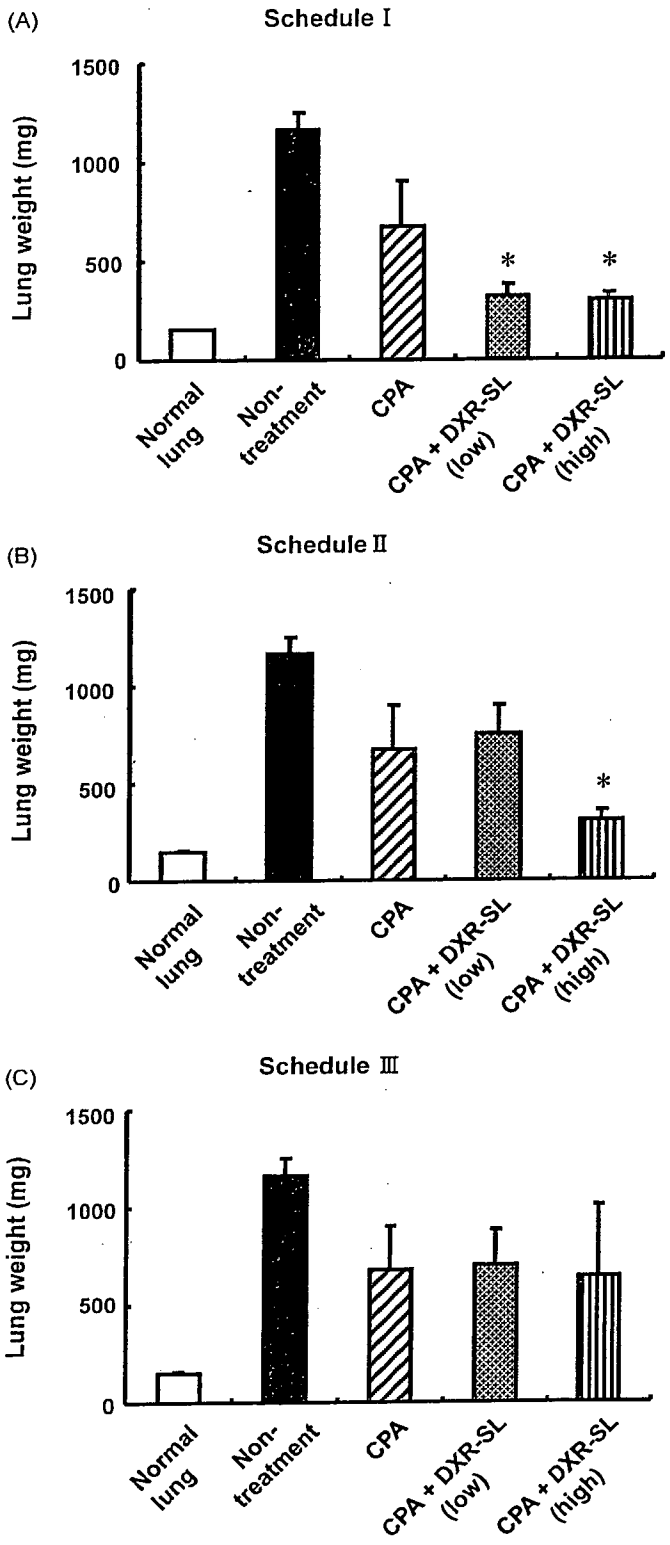

Fig. 4. Effect of the combination of metronomic CPA- and sequential DXR-SL-dosing on lung weight in B16BL6-bearing mice. The dosing schedules used were the same as those described in the legend of Fig. 3: (A) Schedule I (low or high dose of DXR-SL); (B) Schedule II (low or high dose of DXR-SL); (C) Schedule III (low or high dose of DXR-SL). *$p < 0.001$ vs. metronomic CPA-dosing schedule.

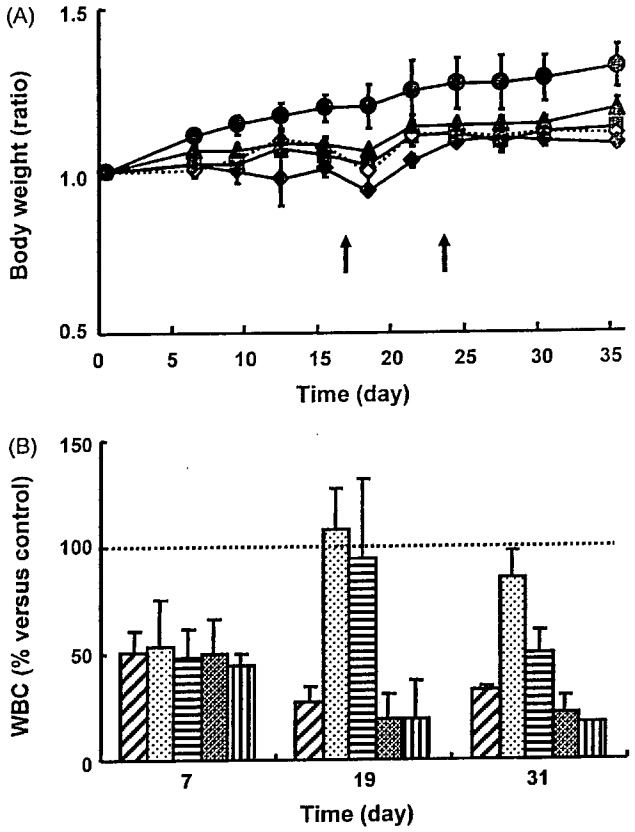

Fig. 5. Toxicity studies for the combination metronomic CPA-dosing plus intravenous administration of DXR-SL. (A) Body weight change. The body weight change expressed as ratio of post-treatment to initial body weight. Control (●), no treatment. CPA (■), 170 mg/kg administered at 6-day intervals. Combination of CPA (170 mg/kg) and low dose DXR-SL (1 mg/kg) administered at 6-day intervals (◇ with dotted line). Combination of CPA (170 mg/kg) and high dose DXR-SL (5 mg/kg) administered at 6-day intervals (◆). DXR-SL (▲), 5 mg/kg administered at 6-day intervals. Arrows indicate time of death for mice treated with combination of CPA (170 mg/kg) and DXR-SL (5 mg/kg). (B) Change in white blood cell number relative to control (no treatment). CPA (▨), 170 mg/kg administered at 6-day intervals. Low dose DXR-SL (▨), 1 mg/kg administered at 6-day intevals. High dose DXR-SL (▤), 5 mg/kg administered at 6-day intervals. Combination of CPA (170 mg/kg) and low dose DXR-SL (1 mg/kg) (▨) administered at 6-day intervals. Combination of CPA (170 mg/kg) and high dose DXR-SL (5 mg/kg) (▤) administered at 6-day intervals.

difficult, the toxicity of the combination therapy of CPA and DXR-SL was examined in not-tumor-bearing mice. In addition, six cycles of the Schedule II combination treatment were employed in the toxicity assessment. At day 35 after initiation of the dosing schedule, the toxicity of the combination therapy was estimated by measuring changes in body weight and WBC number, surrogate markers for treatment-related toxicity.

All combination regimens led to transient weight loss related to growth suppression in treated versus untreated mice (Fig. 5A). Two of the five mice treated with CPA (170 mg/kg) plus the high DXR-SL dose (5 mg/kg) died—one on day 17 and the other on day 24 (Fig. 5A, arrow). This demonstrates that the higher dose of DXR (5 mg/kg) in SL is toxic when combined with CPA. However, tissue weights of treated mice (heart, lung, liver, kidney and spleen) that survived were not different than those of control mice (data not shown).

The metronomic CPA-dosing schedule reduced the number of peripheral WBC (Fig. 5B). DXR-SL also dramatically reduced WBC number, regardless of DXR dose, followed by a rebound in WBC number. The combination regimen (CPA and DXR-SL) reduced the number of WBC, but there was no subsequent rebound in WBC number. The reduction in WBC number with the combination therapy was similar to that observed for the metronomic CPA-dosing schedule. This finding indicates that adding DXR-SL to the metronomic CPA-dosing schedule does not increase the bone marrow toxicity of CPA.

4. Discussion

Metronomic chemotherapy – the frequent administration of an anticancer agent at relatively low, minimally toxic doses with no prolonged drug-free breaks – is a novel approach to the control of advanced cancer. In this study, it was confirmed that the metronomic CPA-dosing schedule exhibited superior therapeutic efficacy in B16BL6-bearing mice, compared with the conventional dosing schedule using the CPA maximum tolerated dose (Fig. 1). Furthermore, the combination of the metronomic CPA-dosing schedule with sequential injections of DXR-SL increased therapeutic efficacy compared to administration of either treatment alone, although the effect was dependent on the schedule and dose of DXR-SL (Figs. 1–3).

Metronomic chemotherapy using CPA is believed to induce apoptosis in the endothelial cells of the growing tumor vasculature (Browder et al., 2000; Kerbel and Kamen, 2004). Thus, it was hypothesized that the metronomic CPA-dosing schedule would increase the permeability of tumor microvessels to macromolecules, including SL, resulting in enhanced accumulation of SL in tumors. Consequently, the therapeutic efficacy of anticancer agents would be enhanced. As expected, the results of the present study showed that some of the combined CPA and DXR-SL dosing schedule had improved therapeutic efficacy (Fig. 3). It should be noted that injection of DXR-SL alone (every 6 days, three times) showed no improvement in MST, regardless of the dose of DXR. Only the high dose of DXR-SL slightly suppressed the growth of cells that had metastasized to the lung (Fig. 2). This result strongly supports the hypothesis that metronomic CPA therapy changes the tumor neovasculature, resulting in enhanced extravasation and subsequent accumulation of SL in tumors. However, the ability of metronomic chemotherapy to enhance the EPR effect remains to be determined.

Interestingly, the improvement was dependent on the dosing schedule, as well as on the DXR-SL dose. Schedule I (low dose of DXR-SL) and Schedule II (high dose of DXR-SL) significantly increased the MST of tumor-bearing mice and inhibited the growth of cells that had metastasized to the lung, compared with the metronomic CPA-dosing schedule (Figs. 3 and 4). In contrast, Schedule III did not increase MST. It is thought that SL, which has a long half-life in circulation, accumulates in solid tumors due to the EPR effect (Jain, 1987; Papahadjopoulos et al., 1991; Wu et al., 1993; Yuan et al., 1995; Forssen et al., 1996; Vaage et al., 1997; Maeda et al., 2000), if the tumor vessels are still permeable. Preclinical and clinical evidence shows that anti-angiogenic therapies normalize the endothelial cells of tumor vessels and consequently decrease vessel permeability (Huber et al., 2005; Jain et al., 2007). These reports describing the biodistribution of SL led to the hypothesis that the metronomic CPA-dosing schedule (an anti-angiogenic therapy) transiently increases tumor vessel permeability and then decreases it as vessels are "normalized". Therefore. It is possible that for Schedule III, according to which DXR-SL is administered 3 days after the first CPA injection, SL accumulation was inhibited, thereby preventing a therapeutic effect (Figs. 3 and 4).

Schedule I (high dose of DXR-SL) resulted in significantly reduced lung weights without any improvement in MST. This apparent inconsistency may be due to enhanced toxicity of the combination of metronomic CPA therapy and intravenous liposomal DXR treatment. Increased toxicity of the combination treatment was supported by the death of two out of five normal mice during six cycles of the combination of CPA and DXR-SL administered at 6-day intervals (Fig. 5A). Furthermore, the combined therapies suppressed weight gain in normal mice. However, it appears that the increased toxicity in this study was not caused by enhancement of the myelosuppressive effects of CPA (Gale, 1985) by the DXR-SL injections (Fig. 5B). Although SL has a long half-life in circulation because of reduced opsonization by serum proteins and lowered recognition by cells of the MPS (Lasic et al., 1991; Torchilin et al., 1994), a fraction of administered SL is ultimately cleared by hepatic macrophages. Daemen et al. (1995, 1997) reported that injection of DXR-SL has a toxic effect on hepatic macrophages, reducing both specific phagocytic activity and cell numbers. Hence, it may be presumed that the toxic effects of CPA and DXR-SL can be either additive or synergistic, resulting in death in some experimental animals.

Other researchers have already demonstrated that the combination of several drugs administered by metronomic dosing with specific antiangiogenic reagents significantly increased the antitumor effects of metronomic dosing (Browder et al., 2000; Klement et al., 2000, 2002; Takahashi et al., 2001; Bello et al., 2001). Recently, Kano et al. (2007) reported that a low dose of transforming growth factor type I receptor (TβR-I) inhibitor promoted accumulation of macromolecules, including nanocarriers (polymeric micelles incorporating DXR), in tumors. TβR-I inhibitor specifically increases the permeability of the tumor neovasculature by decreasing coverage of the endothelium without decreasing endothelial area. This observation clearly suggests that the low dose of TβR-I inhibitor enhances the EPR effect in solid tumors, thereby increasing the therapeutic efficacy of DXR-containing nanocarrier. To the best of our knowledge, this is the first study to demonstrate that the combination of metronomic chemotherapy and liposomal anticancer drug (DXR) treatment increases antitumor effect, presumably by enhancing accumulation of liposomal anti-cancer drugs within the tumor. Thus, the combination of metronomic chemotherapy and liposomal anticancer agents such as Doxil is an innovative strategy in cancer chemotherapy. However, additional studies are needed to determine optimal dosages and treatment schedules to enhance therapeutic efficacy without any adverse effects.

Acknowledgements

We thank Dr. James L. McDonald for his helpful advice in writing the English manuscript. This study was supported by the Kobayashi Fund for Cancer Research and the Knowledge Cluster Initiative from Ministry of Education, Science and Technology.

References

Bartlett, G.R., 1959. Colorimetric assay methods for free and phosphorylated glyceric acids. J. Biol. Chem. 234, 469–471.

Bello, L., Carrabba, G., Giussani, C., Lucini, V., Cerutti, F., Scaglione, F., Landre, J., Pluderi, M., Tomei, G., Villani, R., Carroll, R.S., Black, P.M., Bikfalvi, A., 2001. Low-dose chemotherapy combined with an antiangiogenic drug reduces human glioma growth in vivo. Cancer Res. 61, 7501–7506.

Bolotin, E.M., Cohen, R., Bar, L.K., Emanuel, S.N., Lasic, D.D., Barenholz, Y., 1994. Ammonium sulphate gradients for efficient and stable remote loading of amphipathic weak bases into liposomes and ligandosomes. J. Liposome Res. 4, 455–479.

Browder, T., Butterfield, C.E., Kraling, B.M., Shi, B., Marshall, B., O'Reilly, M.S., Folkman, J., 2000. Antiangiogenic scheduling of chemotherapy improves efficacy against experimental drug-resistant cancer. Cancer Res. 60, 1878–1886.

Daemen, T., Hofstede, G., Ten Kate, M.T., Bakker-Woudenberg, I.A., Scherphof, G.L., 1995. Liposomal doxorubicin-induced toxicity: depletion and impairment of phagocytic activity of liver macrophages. Int. J. Cancer 61, 716–721.

Daemen, T., Regts, J., Meesters, M., Ten Kate, M.T., Bakker-Woudenberg, I.A., Scherphof, G.L., 1997. Toxicity of doxorubicin entrapped within long-circulating liposomes. J. Control. Release 44, 1–9.

Dawson, D.W., Pearce, S.F., Zhong, R., Silverstein, R.L., Frazier, W.A., Bouck, N.P., 1997. CD36 mediates the In vitro inhibitory effects of thrombospondin-1 on endothelial cells. J. Cell Biol. 138, 707–717.

de Fraipont, F., Nicholson, A.C., Feige, J.J., Van Meir, E.G., 2001. Thrombospondins and tumor angiogenesis. Trends Mol. Med. 7, 401–407.

Forssen, E.A., Male-Brune, R., Adler-Moore, J.P., Lee, M.J., Schmidt, P.G., Krasieva, T.B., Shimizu, S., Tromberg, B.J., 1996. Fluorescence imaging studies for the disposition of daunorubicin liposomes (DaunoXome) within tumor tissue. Cancer Res. 56, 2066–2075.

Gale, R.P., 1985. Antineoplastic chemotherapy myelosuppression: mechanisms and new approaches. Exp. Hematol. 13 (Suppl. 16), 3–7.

Gille, J., Spieth, K., Kaufmann, R., 2005. Metronomic low-dose chemotherapy as antiangiogenic therapeutic strategy for cancer. J. Dtsch Dermatol Ges. 3, 26–32.

Grunaug, M., Bogner, J.R., Loch, O., Goebel, F.D., 1998. Liposomal doxorubicin in pulmonary Kaposi's sarcoma: improved survival as compared to patients without liposomal doxorubicin. Eur. J. Med. Res. 3, 13–19.

Guo, N., Krutzsch, H.C., Inman, J.K., Roberts, D.D., 1997. Thrombospondin 1 and type I repeat peptides of thrombospondin 1 specifically induce apoptosis of endothelial cells. Cancer Res. 57, 1735–1742.

Hamano, Y., Sugimoto, H., Soubasakos, M.A., Kieran, M., Olsen, B.R., Lawler, J., Sudhakar, A., Kalluri, R., 2004. Thrombospondin-1 associated with tumor microenvironment contributes to low-dose cyclophosphamide-mediated endothelial cell apoptosis and tumor growth suppression. Cancer Res. 64, 1570–1574.

Huber, P.E., Bischof, M., Jenne, J., Heiland, S., Peschke, P., Saffrich, R., Grone, H.J., Debus, J., Lipson, K.E., Abdollahi, A., 2005. Trimodal cancer treatment: beneficial effects of combined antiangiogenesis, radiation, and chemotherapy. Cancer Res. 65, 3643–3655.

Ishida, T., Maeda, R., Ichihara, M., Irimura, K., Kiwada, H., 2003. Accelerated clearance of PEGylated liposomes in rats after repeated injections. J. Control Release 88, 35–42.

Jain, R.K., 1987. Transport of molecules across tumor vasculature. Cancer Metastasis Rev. 6, 559–593.

Jain, R.K., Tong, R.T., Munn, L.L., 2007. Effect of vascular normalization by antiangiogenic therapy on interstitial hypertension, peritumor edema, and lymphatic metastasis: insights from a mathematical model. Cancer Res. 67, 2729–2735.

Jimenez, B., Volpert, O.V., Crawford, S.E., Febbraio, M., Silverstein, R.L., Bouck, N., 2000. Signals leading to apoptosis-dependent inhibition of neovascularization by thrombospondin-1. Nat. Med. 6, 41–48.

Kano, M.R., Bae, Y., Iwata, C., Morishita, Y., Yashiro, M., Oka, M., Fujii, T., Komuro, A., Kiyono, K., Kaminishi, M., Hirakawa, K., Ouchi, Y., Nishiyama, N., Kataoka, K., Miyazono, K., 2007. Improvement of cancer-targeting therapy, using nanocarriers for intractable solid tumors by inhibition of TGF-beta signaling. Proc. Natl. Acad. Sci. U.S.A. 104, 3460–3465.

Kerbel, R.S., Kamen, B.A., 2004. The anti-angiogenic basis of metronomic chemotherapy. Nat. Rev. Cancer 4, 423–436.

Klement, G., Baruchel, S., Rak, J., Man, S., Clark, K., Hicklin, D.J., Bohlen, P., Kerbel, R.S., 2000. Continuous low-dose therapy with vinblastine and VEGF receptor-2 antibody induces sustained tumor regression without overt toxicity. J. Clin. Invest. 105, R15–R24.

Klement, G., Huang, P., Mayer, B., Green, S.K., Man, S., Bohlen, P., Hicklin, D., Kerbel, R.S., 2002. Differences in therapeutic indexes of combination metronomic chemotherapy and an anti-VEGFR-2 antibody in multidrug-resistant human breast cancer xenografts. Clin. Cancer Res. 8, 221–232.

Klink, T., Bela, C., Stoelting, S., Peters, S.O., Broll, R., Wagner, T., 2006. Metronomic trofosfamide inhibits progression of human lung cancer xenografts by exerting anti-angiogenic effects. J. Cancer Res. Clin. Oncol. 132, 643–652.

Krown, S.E., Northfelt, D.W., Osoba, D., Stewart, J.S., 2004. Use of liposomal anthracyclines in Kaposi's sarcoma. Semin. Oncol. 31, 36–52.

Laquente, B., Vinals, F., Germa, J.R., 2007. Metronomic chemotherapy: an antiangiogenic scheduling. Clin. Transl. Oncol. 9, 93–98.

Lasic, D.D., Martin, F.J., Gabizon, A., Huang, S.K., Papahadjopoulos, D., 1991. Sterically stabilized liposomes: a hypothesis on the molecular origin of the extended circulation times. Biochim. Biophys. Acta 1070, 187–192.

Lawler, J., 2002. Thrombospondin-1 as an endogenous inhibitor of angiogenesis and tumor growth. J. Cell Mol. Med. 6, 1–12.

Li, W., Ishida, T., Okada, Y., Oku, N., Kiwada, H., 2005. Increased gene expression by cationic liposomes (TFL-3) in lung metastases following intravenous injection. Biol. Pharm. Bull. 28, 701–706.

Maeda, H., Wu, J., Sawa, T., Matsumura, Y., Hori, K., 2000. Tumor vascular permeability and the EPR effect in macromolecular therapeutics: a review. J. Control Release 65, 271–284.

Munoz, R., Man, S., Shaked, Y., Lee, C.R., Wong, J., Francia, G., Kerbel, R.S., 2006. Highly efficacious nontoxic preclinical treatment for advanced metastatic breast cancer using combination oral UFT-cyclophosphamide metronomic chemotherapy. Cancer Res. 66, 3386–3391.

Munoz, R., Shaked, Y., Bertolini, F., Emmenegger, U., Man, S., Kerbel, R.S., 2005. Anti-angiogenic treatment of breast cancer using metronomic low-dose chemotherapy. Breast 14, 466–479.

Papahadjopoulos, D., Allen, T.M., Gabizon, A., Mayhew, E., Matthay, K., Huang, S.K., Lee, K.D., Woodle, M.C., Lasic, D.D., Redemann, C., Martin, F.J., 1991. Sterically stabilized liposomes: improvements in pharmacokinetics and antitumor therapeutic efficacy. Proc. Natl. Acad. Sci. U.S.A. 88, 11460–11464.

Safra, T., Muggia, F., Jeffers, S., Tsao-Wei, D.D., Groshen, S., Lyass, O., Henderson, R., Berry, G., Gabizon, A., 2000. Pegylated liposomal doxorubicin (doxil): reduced clinical cardiotoxicity in patients reaching or exceeding cumulative doses of 500 mg/m^2. Ann. Oncol. 11, 1029–1033.

Shaked, Y., Emmenegger, U., Man, S., Cervi, D., Bertolini, F., Ben-David, Y., Kerbel, R.S., 2005. Optimal biologic dose of metronomic chemotherapy regimens is associated with maximum antiangiogenic activity. Blood 106, 3058–3061.

Takahashi, N., Haba, A., Matsuno, F., Seon, B.K., 2001. Antiangiogenic therapy of established tumors in human skin/severe combined immunodeficiency mouse chimeras by anti-endoglin (CD105) monoclonal antibodies, and synergy between anti-endoglin antibody and cyclophosphamide. Cancer Res. 61, 7846–7854.

Tonini, G., Schiavon, G., Silletta, M., Vincenzi, B., Santini, D., 2007. Antiangiogenic properties of metronomic chemotherapy in breast cancer. Future Oncol. 3, 183–190.